nature biomedical engineering

SUPPLEMENTARY INFORMATION

https://doi.org/10.1038/s41551-019-0423-2

In the format provided by the authors and unedited.

Phage-guided modulation of the gut microbiota of mouse models of colorectal cancer augments their responses to chemotherapy

Di-Wei Zheng[1,2], Xue Dong[1,2], Pei Pan[1], Ke-Wei Chen[1], Jin-Xuan Fan[1], Si-Xue Cheng[1] and Xian-Zheng Zhang[1]*

[1]Key Laboratory of Biomedical Polymers of Ministry of Education & Department of Chemistry, Wuhan University, Wuhan, China. [2]These authors contributed equally: Di-Wei Zheng, Xue Dong. *e-mail: xz-zhang@whu.edu.cn

nature biomedical engineering

SUPPLEMENTARY INFORMATION

https://doi.org/10.1038/s41551-019-0423-2

In the format provided by the authors and unedited.

Phage-guided modulation of the gut microbiota of mouse models of colorectal cancer augments their responses to chemotherapy

Di-Wei Zheng[1,2], Xue Dong[1,2], Pei Pan[1], Ke-Wei Chen[1], Jin-Xuan Fan[1], Si-Xue Cheng[1] and Xian-Zheng Zhang[1]*

[1]Key Laboratory of Biomedical Polymers of Ministry of Education & Department of Chemistry, Wuhan University, Wuhan, China. [2]These authors contributed equally: Di-Wei Zheng, Xue Dong. *e-mail: xz-zhang@whu.edu.cn

Table of contents

Methods

Materials. Carboxymethyl-dextran sodium salt (M_w ~10,000) was purchased from TCI. 6-(Boc-amino) hexyl bromide, 2-nitroimidazole (NI), metronidazole and irinotecan (IRT) were purchased from Sigma-Aldrich. DBCO-PEG_{2000}-NH_2 was purchased from Ponsure Biotechnology. 1-Ethyl-3(3-dimethylaminopropyl)carbodiimide (EDC) and N-hydroxysuccinimide (NHS) were purchased from Energy Chemical (Shanghai, China). Oxaliplatin, 5-fluorouracil (5-FU), gemcitabine and paclitaxel were purchased from Aladdin Reagents. Doxorubicin hydrochloride (DOX) was purchased from Zhejiang Hisun Pharmaceutical Co. (China). CB1954 was purchased from Targetmol. 3-Methyladenine, ferrostatin-1, necrostatin-1 and DEVD-CHO were purchased from Selleck Co. ZnO, graphene oxide, and cellulose were purchased from Xfnano (China). Dextran was purchased from Shanghai Yuanye Biotechnology. Roswell Park Memorial Institute (RPMI) 1640 medium, fetal bovine serum (FBS), penicillin–streptomycin and trypsin were provided by Invitrogen (USA). 3-[4,5-Dimethylthiazol-2-yl]-2,5-diphenyltetrazolium-bromide (MTT) was supplied by Beyotime Biotechnology Co. Ltd. (China). Live-dead cell staining kit was purchased from Thermo Fisher Scientific. Transwell® chamber was purchased from Corning Costar.

Preparation of different nanoparticles. The preparation of AuNP, AgNP, C_3N_4 and Fe_3O_4 is detailed as follows.

AuNP: 100 mL 5 mM $HAuCl_4$ was added to 300 mL of ice-cold $NaBH_4$ solution

(2 mM). Then, 50 mL 1% PVA was added during the reduction and stirred for 3 h. The mixture was boiled for 1 h to decompose excess of $NaBH_4$ to obtain final nanoparticles.

AgNP: $AgNO_3$ (0.57 g) was added into 133 mL of dextran T100 (w% = 0.2%) solution. The mixture was irradiated for 2 h with UV-light (12 W) at room temperature. Centrifugation was performed (3920 g, 30 min) to obtain AgNP.

C_3N_4: 10 g of urea was added to 5 mL of ultrapure water. Then the suspension was placed in an alumina crucible and heated to 550 °C with a heating rate of 0.5 °C min^{-1} in a muffle furnace. The temperature of the muffle furnace was maintained for 3 h. Then, the obtained powder was cooled to room temperature and washed with DI water three times. C_3N_4 was collected by filtration and dried at room temperature.

Fe_3O_4: 13.10 g of $FeCl_3 \cdot 6H_2O$ and 6.65 g of $FeCl_2 \cdot 4H_2O$ were mixed in 80 mL of DI water. The solution was stirred under nitrogen for 0.5 h and 45 mL of $NH_3 \cdot H_2O$ was added dropwise at 80 °C. 7.5 g of citric acid in 15 mL of water was introduced after the temperature rose to 95 °C and stirred for 90 min. The solution was dialyzed against water with a dialysis bag (MWCO: 14,000 Da) to obtain a stable magneto fluid solution.

Transmission electron microscopy. To obtain the phage-nanoparticles conjugation, A-phage (10 μL, 1×10^{12} PFU) was co-incubated with D-IDNP for 30 minutes. Then, the mixture was centrifuged (5 min, 3920g) to remove residual nanoparticles and the complexes were resuspended in DI water. To observe the autophagosome, CT26 cells were treated with PBS, IDNP (30 μM), IDNP (30 μM) + *Fn* (1×10^7 CFU) and phage +

IDNP (30 μM D-IDNP + 1×10^7 CFU *Fn* + 1×10^8 PFU A-phage), respectively. After incubated for 4 h, cells were washed with PBS for two times and fixed with 2.5% glutaraldehyde. The TEM images were obtained using a JEOL 2000FX instrument.

Phage-nanoparticles conjugation. L-azidohomoalanine (2 μM) was added to the culture medium. DBCO was modified on the surface of nanoparticles (D-IDNP) through EDC/NHS coupling. Phages or azide-modified phages (A-phage) (10^8 PFU) contained 1% agarose gel (thickness: 8 mm; diameter: 14 mm) were placed in 24-well plates. Then, IR808 labelled D-IDNP was also added to co-incubate for 48 h. The *ex vivo* targeting of A-phage and D-IDNP were observed with Perkin-Elmer In Vivo Imaging System (IVIS).

Construction of a spontaneous tumor model in mice. The CRC model was built on 6-8 week old C57BL/6 mice by using azoxymethane (AOM) and DSS. The mice were intraperitoneally injected with AOM solution (10 mg kg^{-1}) on day 0. On day 7, DSS solution (2.5%) was given to mice as the drinking water and lasted for 7 days. Then, on day 14, the mice were fed back to deionized water for two weeks. On day 28 and day 49, the steps described during day 7 to day 27 were repeated. Fecal samples were collected for 16S rDNA sequencing.

C57BL/6J-*Apc*$^{Min/+}$ mice (male, 8 weeks) were purchased from Nanjing Biomedical Research Institute of Nanjing University. After two weeks of normal feeding, their fecal samples were collected for sequencing.

Chemoresistance of CRC cell lines. CT26 cells, HT29 cells and HCT116 cells were seeded on 24-well plates with a density of 1×10^5 cells per well in the growth medium.

After that, the CRC cells were co-cultured with *Fn* (1×10^7 CFU) and a particular chemotherapeutic agent (OXA (126 μM), 5-Fu (800 μM), DOX (0.5 μM), IRT (30 μM), GEM (10 μM), PTX (12 μM) and CB1954 (50 μM)) in 1640 medium containing 10% FBS for 48 h. The effect of *Fn* on rescuing CRC cells from chemotherapeutic agents induced cell death was estimated by MTT assay.

For comparison, CRC cells and a particular chemotherapeutic agent were added in the down chamber of 24-well transwell (Corning Costar, USA) filters, while *Fn* were placed on the up chamber. After incubation for 48 h, the effect of *Fn* on rescuing CRC cells from chemotherapeutic agents induced cell death was estimated by MTT assay.

500 μL MTT (5 mg mL^{-1}) was added into each well and co-incubated for another 4 h. The culture medium in each well was replaced with DMSO (750 μL). The absorbance at 570 nm was measured with SpectraMax i3x multi-mode detection platform. The relative cell viability was counted according to the following formula: cell viability (%) = $(OD_{570(sample)}/OD_{570(control)}) \times 100\%$.

Anti-cancer effects of butyrate on CRC cell lines. CT26 cells, HT29 cells and HCT116 cells were cultured on 96-well plates with a density of 1×10^4 cells per well in the growth medium. Butyrate solutions with gradient concentrations (C_{max} = 64 mM; C_{min} = 0.25 mM) were added into each well and incubated for 48 h. Subsequently, MTT (5 mg mL^{-1}) was added into each well and co-incubated for another 4 h. The cultured medium in each well was replaced with 150 μL DMSO. The relative cell viability was assessed by MTT assay.

***In vitro* cytotoxicity of *Cb*.** *Cb* was inoculated in BHI broth. To inhibit the butyrate generation of *Cb*, neutral red (0.5 mM) was co-incubated with *Cb*. Once cultures reached mid-log phase (OD600 ~0.25), the bacteria were harvested from 500 μL of culture medium by centrifugation, and the supernatant containing secreta of *Cb* was collected. The bacteria were resuspended in 500 μL of BHI broth. Different molecular weight components of secreta (Mw>3,000 and Mw<3,000) were obtained by ultrafiltration (15min, 3920 g). These components were dissolved in 500 μL of BHI broth. CT26 cells were seeded on 24-well plates with a density of 1×10^5 cells per well. 24 h later, bacterial components (500 μL) were added to CT26 cells. After being incubated for 48 h, MTT assay was used to assess the cell viability.

Detection of *Fn* induced cancer autophagy. CT26 cells, HT29 cells and HCT116 cells were cultured on 6-well plates with a density of 1×10^5cells per well and were transfected with GFP-LC3B plasmid. Then, CRC cells were treated with PBS, D-IDNP (30 μM), D-IDNP (30 μM) + *Fn* (1×10^7 CFU) and phage + IDNP (30 μM D-IDNP + 1×10^7 CFU *Fn* + 1×10^8 PFU phages), respectively, and co-incubated for 4 h. After that, GFP–LC3 dots were analyzed using confocal microscopy.

The effect of various inhibitors on *Fn* induced cancer autophagy. CT26 cells were seeded on 24-well plates with a density of 1×10^5 cells per well in the growth medium. After that, the cells were co-cultured with *Fn* (1×10^7 CFU) and a particular inhibitor (3-MA (60 μM) (autophagy inhibitor), Fer-1 (60 nM) (ferroptosis inhibitor), Nec-1 (490 nM) (necroptosis inhibitor), and Ac-DEVD-CHO (100 nM) (apoptosis inhibitor))

in 1640 medium containing 10% FBS for 48 h. MTT assay was used to assess the inhibition effect of the inhibitor on *Fn* induced cancer autophagy.

To evaluate the effect of inhibition of Myd88 or TLR4 on autophagy, CT26 cells were transfected by siRNA-Myd88 or siRNA-TLR4, and then seeded on 24-well plates with a density of 1×10^5 cells per well in 1640 medium containing 10% FBS for 24 h. After that, the cells were co-cultured with *Fn* (1×10^7 CFU) for 48 h, and then examined by MTT assay.

Flow cytometry. Cells were cultured on 6-well plates with a density of 1×10^5 cells per well and were constitutively transfected with mCherry-GFP-LC3. After being treated with PBS, IDNP (30 μM), IDNP (30 μM) + *Fn* (1×10^7 CFU) and phage + IDNP (30 μM IDNP + 1×10^7 CFU *Fn* + 1×10^8 PFU phage) respectively, and co-incubated for 4 h, flow cytometry was used to analyze autophagy effect of cells. Generally, cells were first gated on FSC/SSC. Singlet cells were usually gated using FSC-H and FSC-A. GFP and mCherry gating were performed on the live cell population. The FL1/FL2 ratio was determined by FlowJo software.

***In vitro* circulating device for simulating the physiological environment.** A circulating device was designed to stimulate the physiological environment of intestinal tract. FITC labeled *Fn* and *E. coli* were immobilized in a 1% agarose gel (10^7 CFU of *bacteria in* 18 mm × 5 mm × 3mm sized hydrogel cuboid). The flow velocity of the artificial intestinal juice (100 mM KH_2PO_4 + 20 g L^{-1} pancreatin, pH 6.8) was 0.85 cm/s, and the viscosity of the artificial intestinal juice was 30 cp. The rhodamine B labeled A-phage containing solution was cycled for 6 h. The

fluorescence accumulation was observed with Perkin-Elmer IVIS. Then, the circulating fluid was replaced with simulated intestinal juice containing IR808 encapsulated D-IDNP (0.5 mg mL^{-1}). After 6 h of circulation, the accumulation of IR808 encapsulated D-IDNP was observed with Perkin-Elmer IVIS.

***In vivo* tumor targeting of A-phage + D-IDNP.** For the orthotopic tumor model, luciferase transfected CT26 tumor cells were transplanted in the cecum of BALB/c mice. *Fn* (1×10^8 CFU per mice) was given 24 h before the post-treatment. 100 μL Cy5 labeled A-phage (1×10^{11} PFU) was intragastrically administrated into mice. 15 min later, 100 μL IR808 labeled D-IDNP (296 mg kg^{-1}) was orally administered. To test the tumor targeting of phage-guided nano-therapeutic system, mice were treated with D-IDNP (296 mg kg^{-1}) + A-phage (1×10^{11} PFU) and IDNP (296 mg kg^{-1}) + phage (1×10^{11} PFU), respectively. The fluorescence of nanoparticles (IR808) and phages (Cy5), as well as the bioluminescence of tumors, were imaged with IVIS system at different time points. After 24 h of *in vivo* fluorescence imaging, mice were sacrificed, and tumors of these mice were collected for *ex vivo* imaging.

Biosafety in piglet and murine models. The female BALB/c mice were randomly assigned into 4 groups (n = 3). Then, mice were injected with 100 μL PBS (*i.p.*), IRT (0.17 mg kg^{-1}, *i.p.*), IDNP (296 mg kg^{-1}, *i.p.*) and the mixture of IDNP (296 mg kg^{-1}, *i.p.*) + phage (1×10^{11} PFU, *i.p.*), respectively. 24 h later, mice were sacrificed and their small intestines were collected for pathological analysis. Macrophage inflammatory protein activity (MIP-β), MDA content, and myeloperoxidase activity (MPO) were also determined. The piglets were randomly divided into 2 groups (n = 3). Then,

piglets were gavaged with phages (10^{12} PFU) and INP (296 mg kg^{-1}). 1 week later, blood samples were collected for hematological examination (WBC, Lymph, Mid, Gran and Plt), liver function test (ALT, AST and GGT), kidney function test (UREA, CRE and TBIL) and anaphylactic effect evaluation (IgG, IgE and histamine). At different time points, fecal samples of piglets were gathered for 16S rDNA sequencing.

Fluorescence labelling of bacteria and phages. 0.1 mg FITC was added to the suspension of bacteria (1×10^8 CFU mL^{-1} in PBS). The reaction was carried out for at 37 °C. 12 h later, the mixture was centrifuged (5 min, 3920g) to obtain FTIC-labelled bacteria. To obtain Cy5-labelled phages, 0.1 mg Cy5 NHS ester was added to the suspension of phages (1×10^{12} PFU mL^{-1} in PBS). The reaction was kept at 37 °C for 12 h. The residual Cy5 NHS esters was removed with ultrafiltration (Mw = 100 kDa) for 5 min at a speed of 3920 g.

Abdominal imaging window for tumor observation. A titanium ring was designed and fabricated with 3D printing. The round-shaped coverslip was bonded on the titanium ring with 3M Vetbound. This device was coated with $PLL_{(20)}$-$g_{[3.5]}$-$PEG_{(2)}$ (0.1 mg mL^{-1}). After that, this device was placed on the abdomen of tumor bearing mice. At the same time, the orthotopic tumor model was constructed. Then, the tumor progression was observed over time by a stereomicroscope at different time points. On the day 0 (5 days after the window implantation), mice were gavaged with 1×10^8 CFU *Fn*, and randomly divided into 6 groups with 5 mice in each group. 100 μL PBS, 100 μL antibiotic cocktail (200 mg kg^{-1} metronidazole, 250 mg kg^{-1} ampicillin, 250mg

kg^{-1} vancomycin), 100 μL IDNPs (296 mg kg^{-1}) and A-phages + D-IDNPs (100 μL D-IDNP, 296 mg kg^{-1} + 100 μL A-phage, 1×10^{11} PFU) were intragastrically administered every week. For mice in the FOLFIRI group and IRT group, 100 μL of chemotherapeutics (30 mg kg^{-1} 5-fluorouracil, 90 mg kg^{-1} leucovorin and 16 mg kg^{-1} IRT, *i.v.*) and 100 μL 16 mg kg^{-1} IRT (*i.v*) were given once a week.

Transcriptome sequencing. CT26 cells were treated with PBS, IDNP (30 μM), IDNP (30 μM) + *Fn* (1×10^9 CFU) and IDNP + phage (30 μM D-IDNP + 1×10^9 CFU *Fn* + 1×10^{10} PFU A-phage), respectively. After incubated for 4 h, the cells were washed with PBS for two times and collected for further experiments. The high-throughput sequencing was performed in Majorbio BioTech Co., Ltd. The data were analyzed online with I-Sanger Cloud Platform.

Changes of SCFA levels. Fecal samples of tumor bearing mice were collected before and after different treatments. 24 h after the administraion of *Fn* (10^8 CFU), a particular agent (PBS, antibiotics cocktail (metronidazole 200 mg kg^{-1}, ampicillin 250 mg kg^{-1}, vancomycin 250 mg kg^{-1}), irinotecan (16 mg kg^{-1}), FOLFIRI (5-Fu 30 mg kg^{-1}, leucovorin 90 mg kg^{-1}, IRT 16 mg kg^{-1}), IDNP (296 mg kg^{-1}), and D-IDNP + A-phage (296 mg kg^{-1} D-IDNP and 10^{11} PFU A-phage)) was given. The therapeutics were administered once a week. These fecal samples were collected for 16S rDNA sequencing and GC–MS analysis.

For the measurement of fecal SCFA levels, 200 mg of frozen feces was vortexed for 1 min in 1% HCl. Homogenized samples were centrifuged at 2,350 g for 30 s. The supernatant was acidified to pH 0 with HCl. Each sample was partitioned into four

aliquots and extracted at 4 °C with an equal volume of diethyl ether. Samples were incubated with 1-tertbutyl-dimethylsilyl-imidazole at 60 °C for 30 min before GC-MS analysis (Agilent 7890A, equipped with a DB-FFAP capillary column. The data were analyzed with FID Chem Station (G1701EA.02.00.493) and ACD/Spectrus Processor 2015. The concentration of butyrate in the medium was also examined in the same manner.

Structural changes of gut microbiota. Bacterial genomic DNA was extracted from mouse fecal samples using the MoBio PowerSoil Kit. The V4 regions of the 16S rDNA gene were PCR amplified using barcoded universal primers. The PCR reaction was set up in triplicate, and the PCR product was purified using a PCR purification kit. The high-throughput sequencing was performed in Majorbio BioTech Co., Ltd. The data were analyzed on the free online platform of I-Sanger Cloud Platform.

Fluorescence in situ hybridization (FISH) assay in CRC tissues. The tissue microassay was purchased from Biomax. All human tissues are collected under IRB and HIPPA approved protocols. All animal tissues are collected under IACUC protocol. All samples have been tested negative for HIV and Hepatitis B or their counterparts in animals, and approved for commercial product development. Then, *Fn* in the tumor tissues was labeled with a *Fusobacterium* 16S rDNA-directed probe (5'-CTA ATG GGA CGC AAA GCT CTC -3'). After that, Cy5-labeled phages were added to the tissue samples and incubated for 4 h. The colocation analysis was performed with Image J software.

CT imaging, MRI imaging and PET/CT imaging. The intratumoral calcification of

orthotopic implantated CT26 tumor bearing mice was investigated by μ-CT (PerkinElmer, Quantum GX) and 7.0 T MRI (BioSpec 70/20USR). The tumor growth of *Apc*$^{Min/+}$ mice was observed by PET (Trans-PET BioCaliburn-700).

Antibodies for western blot analysis and immunofluorescence. Anti-cleaved caspase3 (GB11009), anti-caspase9 (GB11053-1), anti-LC3A/B (GB11124) and anti-P62 (GB11531) rabbit polyclonal monoclonal antibodies from Servicebio. Anti-Ki67 monoclonal antibody [sp6] was purchased from Genetex.

a

	1	2	3	4	5	6	7	8	9	10
A	Cancerous	Paracancerous	Cancerous	Paracancerous	Cancerous	Paracancerous	Cancerous	Paracancerous	Paracancerous	Paracancerous
B	Cancerous	Paracancerous	Cancerous	Paracancerous	Cancerous	Paracancerous	Cancerous	Cancerous	Cancerous	Paracancerous
C	Cancerous	Paracancerous	Cancerous	Paracancerous	Cancerous	Paracancerous	Cancerous	Paracancerous	Cancerous	Paracancerous
D	Cancerous	Paracancerous	Cancerous	Paracancerous	Cancerous	Paracancerous	Cancerous	Paracancerous	Cancerous	Paracancerous
E	Cancerous	Paracancerous	Cancerous	Paracancerous	Cancerous	Paracancerous	Cancerous	Paracancerous	Cancerous	Paracancerous
F	Cancerous	Paracancerous	Cancerous	Paracancerous	Cancerous	Paracancerous	Cancerous	Paracancerous	Cancerous	Paracancerous
G	Cancerous	Paracancerous	Cancerous	Paracancerous	Cancerous	Paracancerous	Cancerous	Paracancerous	Cancerous	Paracancerous

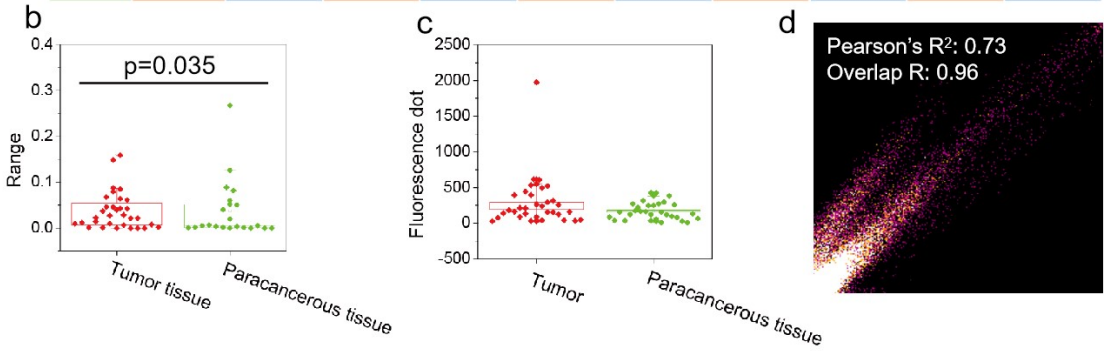

Supplementary Fig. 1 | Information of the tissue sample. (**a**) Sample information of tissue microarray. Detailed patient information is listed in Supplementary Table 6. (**b**) Quantitative analysis of *Fn* content in cancerous and paracancerous tissues. The mean fluorescence intensity of samples was calculated with Image J. (**c**) Quantitative analysis of P2 phages content in cancerous and paracancerous tissues. The number of fluorescence-positive spot was counted with Image J. (**d**) Fluorescence co-localization analysis of P2 phages and *Fn* in clinical tumor samples. A high Mander overlap coefficient of 0.96 was calculated by using Image J with the fluorescence co-localization plug. Significance between two groups was calculated by using two-tailed Student's t test. Definition of boxplots: line inside box: mean; box limits: quartiles: 25th percentile (lower), 75th percentile (upper); coefficient: 1.

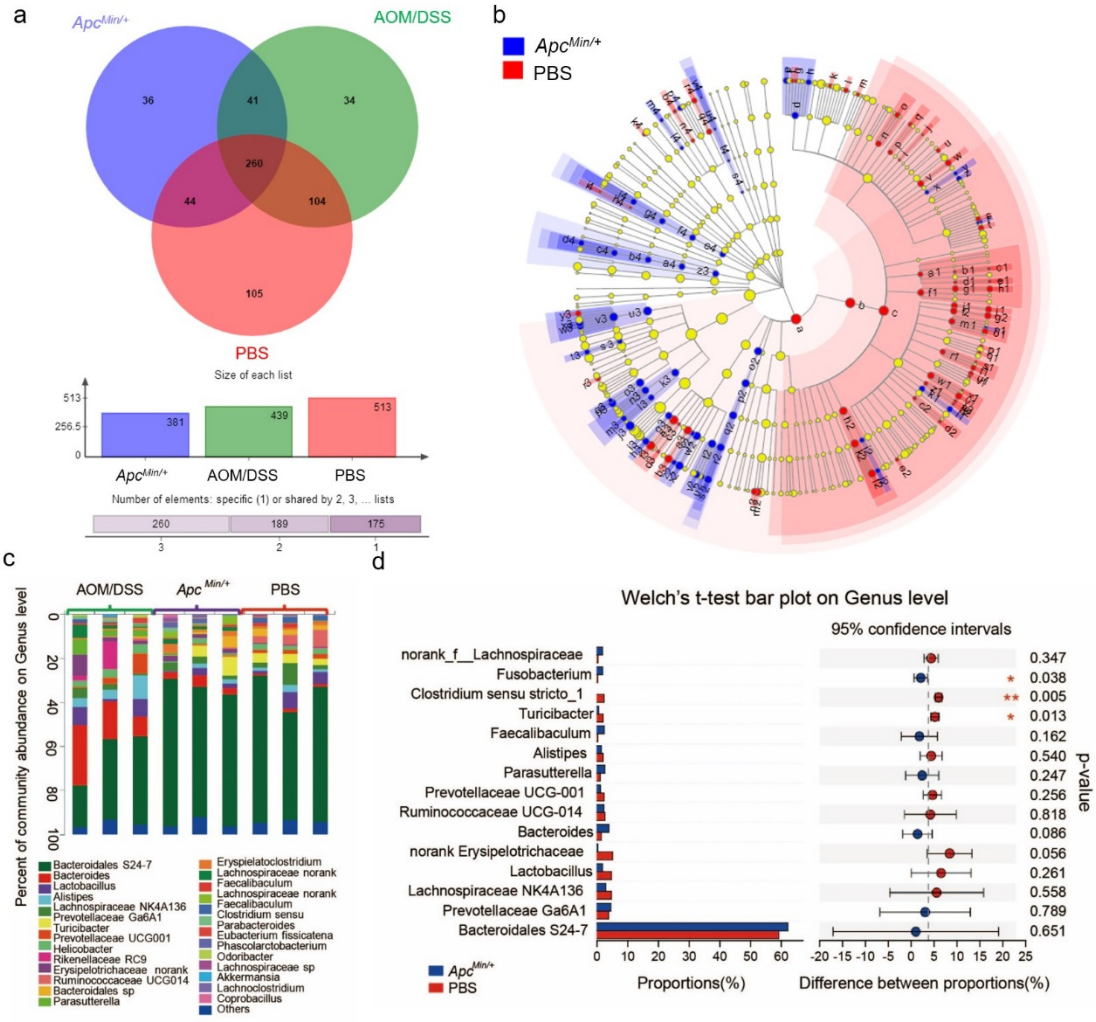

Supplementary Fig. 2 | Community structures of microbes in healthy and cancer mice. (**a**) Venn diagram of identified fecal bacterial strains in healthy C57BL/6J mice and mice models including colitis-associated cancer (AOM/DSS) and spontaneous colonic neoplasms (C57BL/6J-*Apc*$^{Min/+}$ mice). A loss of OTU abundance could be found in *Apc*$^{Min/+}$ mice and AOM/DSS treated mice. Three biological replicates are shown. (**b**) LEfSe (linear discriminant analysis effect size) for analyzing the differential microbes between control group and *Apc*$^{Min/+}$ mice by using non-parametric factorial Kruskal-Wallis (KW) sum-rank test. The nodes represent taxa enriched in wild type (red) or *Apc*$^{Min+/-}$ (blue) 10-week fecal microbiota. The

yellow nodes represent insignificantly enriched taxa. Each ring represents the next lower taxonomic level (kingdoms through genus). The diameter of each circle represents the relative abundance of the taxon. The letter meaning is listed in Supplementary Table 3. (**c**) Genus-level microbial composition of the feces of health C57BL/6J mice, as well as C57BL/6J mice and *Apc*$^{Min/+}$ C57BL/6J mice with AOM/DSS chemically induced colorectal primary tumors. (**d**) Genus level analysis of significant difference bacterial species between two groups. Wilcoxon rank-sum test was performed (n = 3 for each group). Significantly reduced *Clostridium* level and increased *Fusobacterium* proportion could be found.

Supplementary discussion 1. Fecal samples from *Apc*$^{Min/+}$ mice and AOM/DSS treated mice were collected and analyzed. The proportion of 30 most abundant bacterial genera is listed in Supplementary Fig. 2c. In AOM/DSS-treated mice, negligible changes of *Fn* and *Cb* were noticed. Thus, *Apc*$^{Min+/-}$ mice was used for further studies. A marked structural segregation in gut microbiota between *Apc*$^{Min+/-}$ mice and healthy mice was observed. Furthermore, different species between *Apc*$^{Min/+}$ mice and healthy mice were identified by using Welch's t-test. As shown in Supplementary Fig. 2d, significantly increased *Fusobacterium* content, together with decreased *Clostridium sensu stricto* abundance was observed only in *Apc*$^{Min/+}$ transgenic mice.

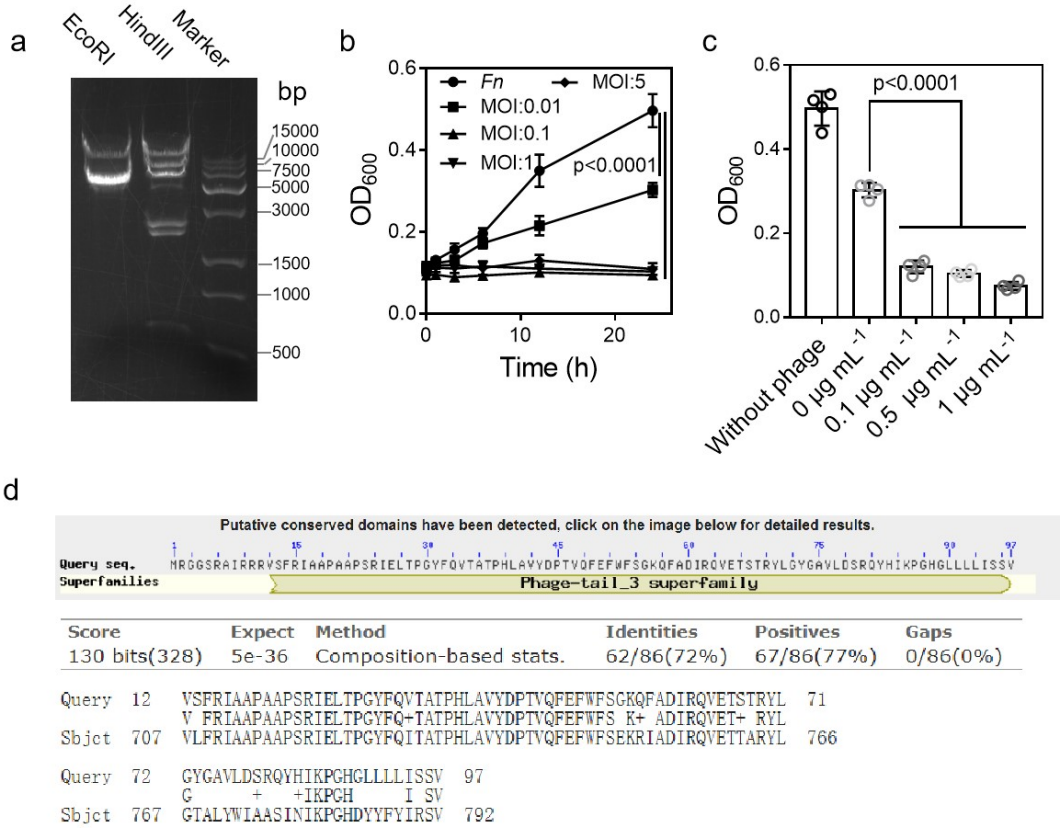

Supplementary Fig. 3 | Characterization of P2 phages. (a) Bands of the digestion of P2 phages with HindIII and EcoRI used for genome size determination. The genome size of P2 phages was calculated to be around 45 kbp. (**b**) Growth curves of *Fn* in the absence or presence of different content of phages. Phages were added at different MOIs (from 0.01 to 5) to *Fn* under early exponential growth phase (OD600 ~0.1). The P2 phages could strongly inhibit the growth of *Fn* and produce homogenous plaque characteristics in the solid medium. Four biological replicates are shown. (**c**) The influence of mitomycin C on the lysis feature of P2 phages. A facilitated lytic process of *Fn* (ATCC 10953) was induced by different concentrations of mitomycin C (from 0 to 1 μg mL^{-1}). Four biological replicates are shown. (**d**) The graphical summary of conserved domains identified on the query sequence. The

deduced protein (Query) was compared with putative tail tip assembly protein (Sbjct) of *Enterobacteria* phage cdtI. A small fragment of DNA (350 bp) was sequenced with rolling circle amplification. An open reading frames (ORF) was identified by using ORF Finder (http://www.bioinformatics.org). A small peptide containing 97 amino acid (aa) was identified. The fragment containing aa12-aa97 was classified into phage-tail 3 superfamily (E value = 6.46×10^{-27}).

Supplementary discussion 2. As shown in Supplementary Fig. 3b, P2 phages could hardly reach complete lysis. These observations imply that P2 phages are temperate phages or the optimal conditions for infection were not achieved. Subsequently, the influence of mitomycin C on the lysis feature of P2 phages was tested (Supplementary Fig. 3c). A facilitated lytic process of *Fn* (ATCC 10953) was induced by mitomycin C with different concentrations (from 0.1 to 1 μg mL^{-1}). Mitomycin C treatment might cause a shift from the lysogenic to the lytic response, indicating P2 phages might be temperate phages that could be reproduced using both the lytic and the lysogenic cycles. A small fragment of DNA (350 bp) was sequenced with rolling circle amplification (Supplementary Fig. 3d). An open reading frame (ORF) containing 97 amino acids was identified by using ORF Finder. The fragment containing aa12-aa97 was classified into phage-tail 3 superfamily (E value = 6.46×10^{-27}). This ORF encoded peptide had 72% identity with the putative tail tip assembly protein of *Enterobacteria* phage cdtI. However, the phages are not active in *Enterobacteria*. Neither identity nor homology was found with any other reported sequences.

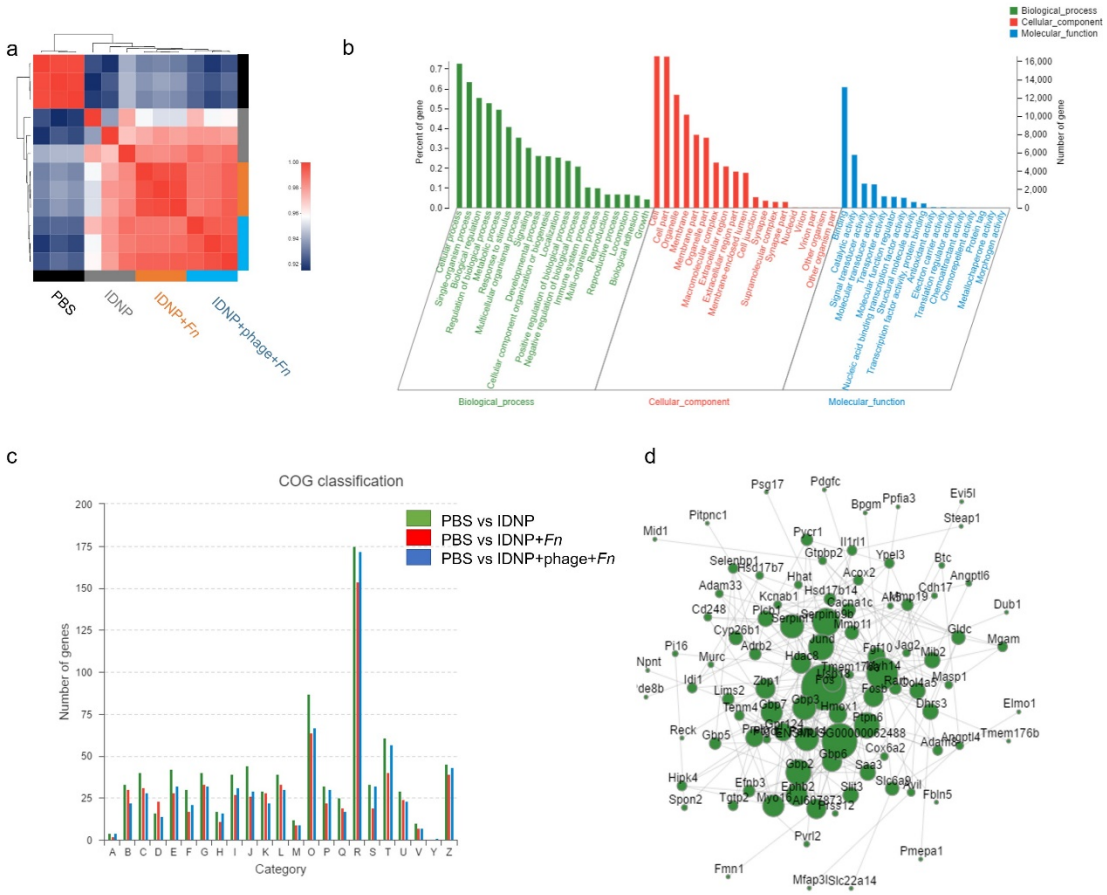

Supplementary Fig. 4 | Transcriptomics analysis of phage-guided nano-therapeutic system. (**a**) Transcriptional correlation among PBS, IDNP, IDNP + *Fn* and IDNP + phage + *Fn* treated CT26 cells. Three biological replicates are shown. (**b**) GO analysis of identified genes. (**c**) GOC enrichment analysis of differential expressed genes among PBS, IDNP, IDNP + *Fn* and IDNP + phage + *Fn* treated groups. GOC items are detailed listed in Supplementary Table 4. (**d**) STRING protein-protein interaction networks for system-wide understanding of cellular function proteins between IDNP + *Fn* and IDNP + phage + *Fn* treated groups.

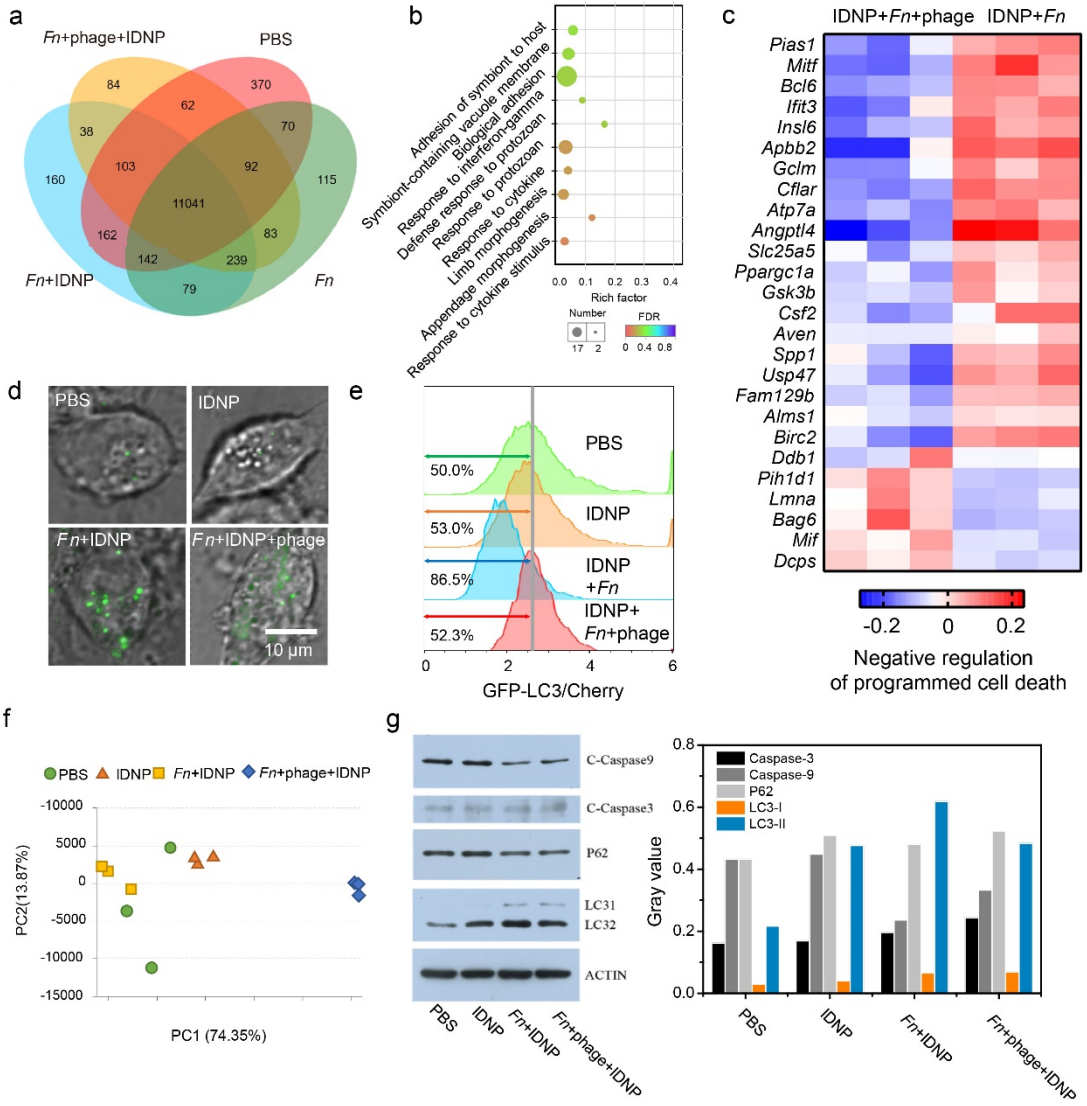

Supplementary Fig. 5 | Mechanism study of phage-guided bio/abiotic hybrid nano-system in treating CRC. (**a**) Venn diagram of identified genes in CT26 cells after treated with PBS, IDNP, *Fn* + IDNP or *Fn* + IDNP + phage. (**b**) Study on potential gene pathway involved in the response of *Fn* induced multidrug resistance. Pathway analyses were performed using GO enrichment tools. Significance between two groups was calculated by using FDR. (**c**) Differential gene expression heat maps of identified genes that involved in the pathway of negative regulation of programmed cell death. Pathway analyses were performed using GO pathway analysis. Three

biological replicates are shown. (**d**) Fluorescence imaging of GFP-LC3-transfected CT26 cells after treated with PBS, IDNP, *Fn* + IDNP or *Fn* + IDNP + phage. Green fluorescent dots in the cytoplasm indicated the formation of autophagosome. Five images per group were taken. Experiments were repeated three times. (**e**) Flow cytometry for quantification of GFP-LC3/mCherry ratio of live CT26 cells expressing tandemGFP-mCherry-LC3 with various treatments. GFP-LC3/mcherry ratio showed autophagy occurrence. Experiments were repeated three times. (**f**) Principal component analysis (PCA) of gene expression in PBS, IDNP, *Fn* + IDNP or *Fn* + IDNP + phage treated CT26 cells. (**g**) Western blot assay on the expression of cleavage caspase3, cleavage caspase9, P62, LC3-I, LC3-II and actin in CT26 cells treated with PBS, IDNP, *Fn* + IDNP or *Fn* + IDNP + phage. Significance between two groups was calculated by using ANOVA with Tukey post hoc (e). The mean values and S.D. are presented.

Supplementary discussion 3. A total of 12,840 genes were analysed, and an absolute fold change > 1.5 with a p value < 0.05 was set as a threshold to define the differentially expressed gene (Supplementary Fig. 4a). First of all, differentially expressed genes between IRT group and *Fn* co-incubation group were annotated with Gene Ontology (GO) enrichment analysis. As shown in Supplementary Fig. 4b, these genes were mainly associated with microbial adhesion and immune responses. Based on this result, we speculated that the biological effect of *Fn* on CRC cells might be directly mediated by the surface contact. In the non-contact culture, the chemoresistance mediated by *Fn* was nearly prevented.

As shown in Supplementary Fig. 4c, after phage treatment, anti-apoptosis associated genes in CT26 cells appeared in the heat map. Among 55 differentially expressed genes in the cluster of negative regulation for programmed cell death, 14 genes were up-regulated and 31 genes were down-regulated. Most chemotherapy drugs currently used in clinical oncology have been closely linked to cell apoptosis. As shown in Fig. 2i, in the GO term of "regulation of autophagy", up-regulation of anti-autophagy genes and down-regulation of pro-autophagy genes were observed after phage treatment. From these results, we speculated that *Fn* might prevent CRC cells from chemotherapy induced apoptosis *via* inducing protective autophagy.

To confirm this mechanism, GFP-LC3 transgenic CT26 cells were used to visualize autophagy in cultured cells. As shown in Supplementary Fig. 5d and Supplementary Fig. 5e, chemotherapy treatment had a negligible effect on autophagy. The number of GFP-positive small vesicles increased after co-incubated with *Fn*. At

the same time, GFP-LC3 protein was degraded gradually, and resulted in the decreased cytoplasmic green fluorescence intensity.

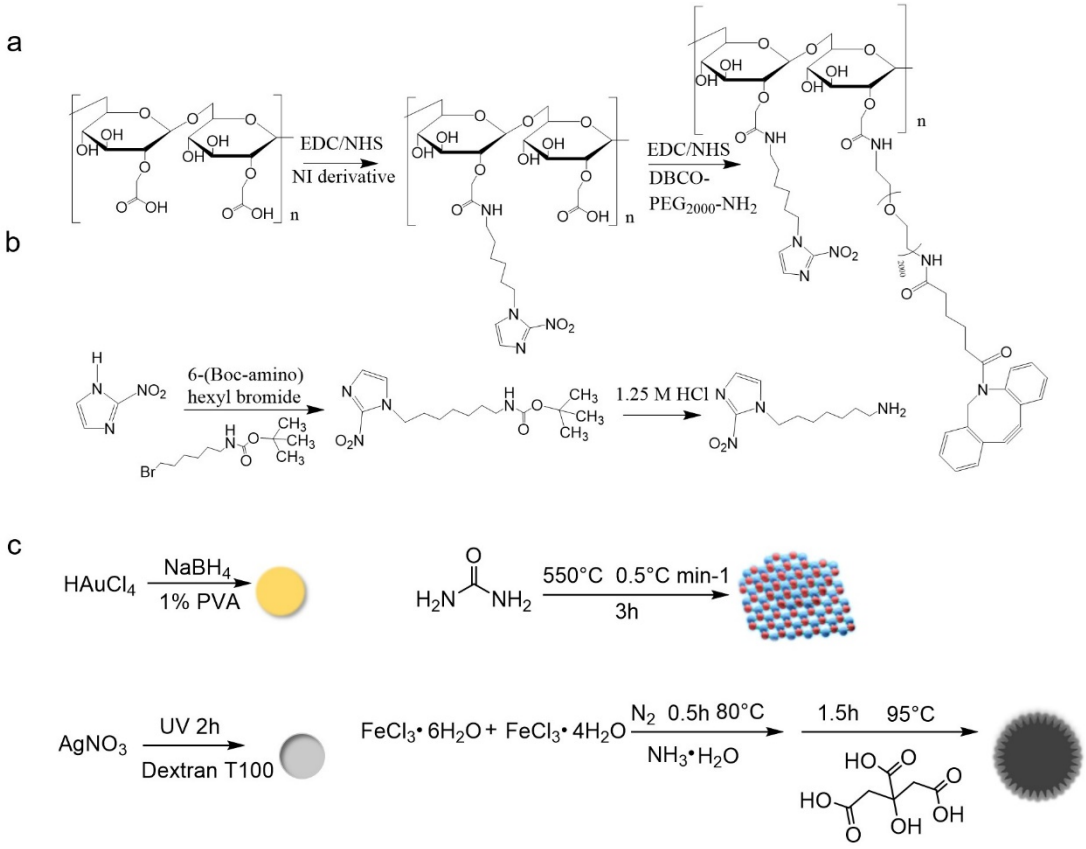

Supplementary Fig. 6 | Preparation of various nanoparticles. (**a**) The synthesis of NI derivative. (**b**) The synthesis of amphiphilic NI-derivative-grafted dextran. (**c**) The preparation of AuNP, C_3N_4 nanoparticles, AgNP and Fe_3O_4 nanoparticles.

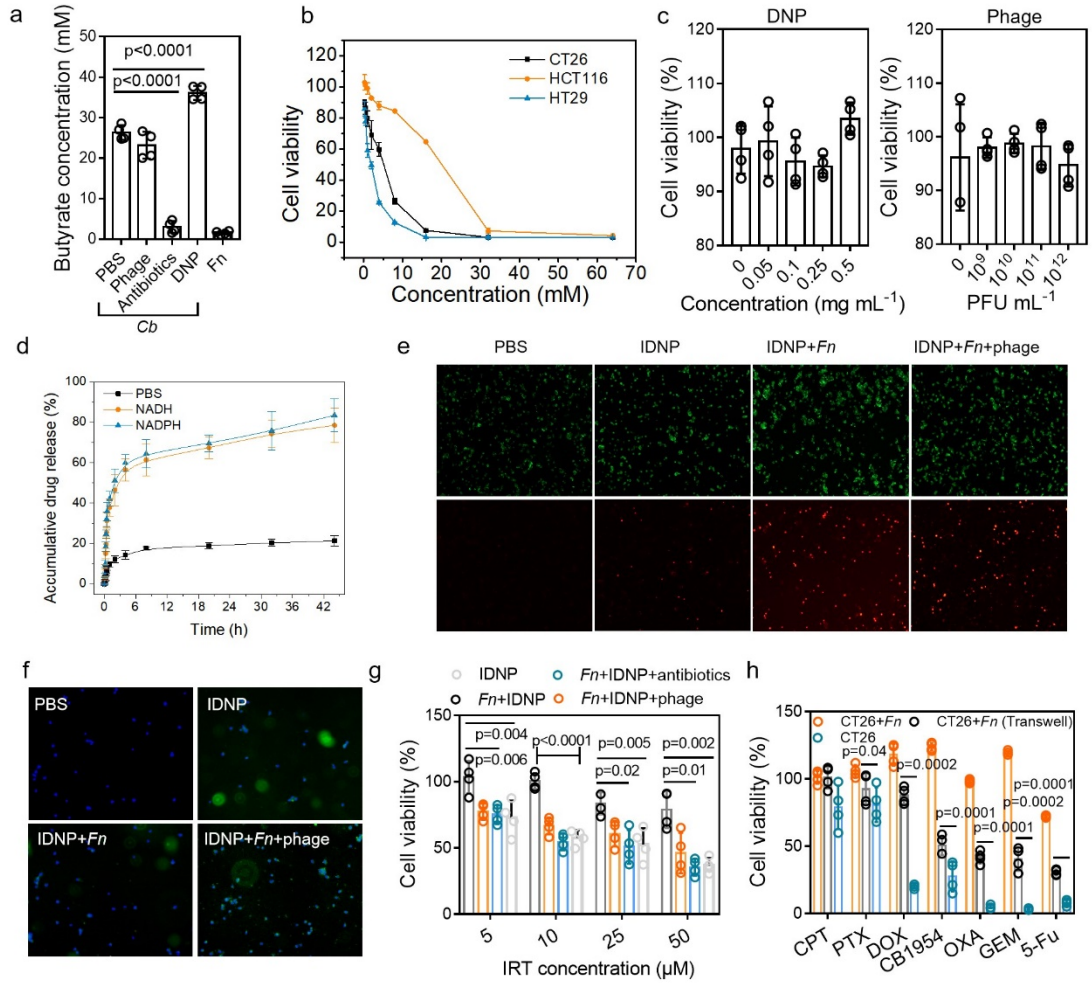

Supplementary Fig. 7 | *In vitro* cell experiments of phage-guided bio/abiotic hybrid nano-system in treating CRC. (**a**) Effects of phages, DNP and antibiotics on the butyrate generation capacity of *Cb*. Four biological replicates are shown. (**b**) *In vitro* anti-cancer effect of butyric acid with various concentrations on CRC cells. Experiments were repeated three times. Four biological replicates are shown. (**c**) Biosafety of phages or DNP in CT26 cells. Four and three biological replicates are shown, respectively. Experiments were repeated three times. (**d**) IRT release curve of IDNP in response to NADH (50 μM) and NADPH (50 μM). IDNP was NAD(P)H-responsive polymeric nanoparticles. The increased NAD(P)H

concentration accelerated the drug release. Experiments were repeated three times. (**e**) Live/dead cell staining of CT26 cells after treated with IDNP, IDNP + *Fn* and phage + IDNP + *Fn*. The green (calcein AM) stained live cells, and red (propidium iodide) fluorescence stained dead cells. Autophagy also improved the affinity of cells towards PI staining. Five images per group were taken. (**f**) Tunel assay of CT26 cells after treated with PBS, IDNP, *Fn* + IDNP or *Fn* + IDNP + phage. Green fluorescence represented cell apoptosis. Five images per group were taken. (**g**) *In vitro* anti-cancer effects of PBS, IDNP, *Fn* + IDNP or *Fn* + IDNP + phage in CT26 cells. The antibiotics treatment inhibited the *Fn*-mediated protective autophagy in CT26 cells. The same dose of IRT is controlled between different materials. Four biological replicates are shown. Experiments were repeated three times. (**h**) The effect of *Fn* on rescuing CT26 cells from chemotherapeutic agents induced cell death. Transwell chamber was used to demonstrate that the protective effect of *Fn* towards CT26 cells was contact-dependent. Four biological replicates are shown. Experiments were repeated three times. Significance between two groups was calculated by using ANOVA with Tukey post hoc (a, g). The mean values and S.D. are presented.

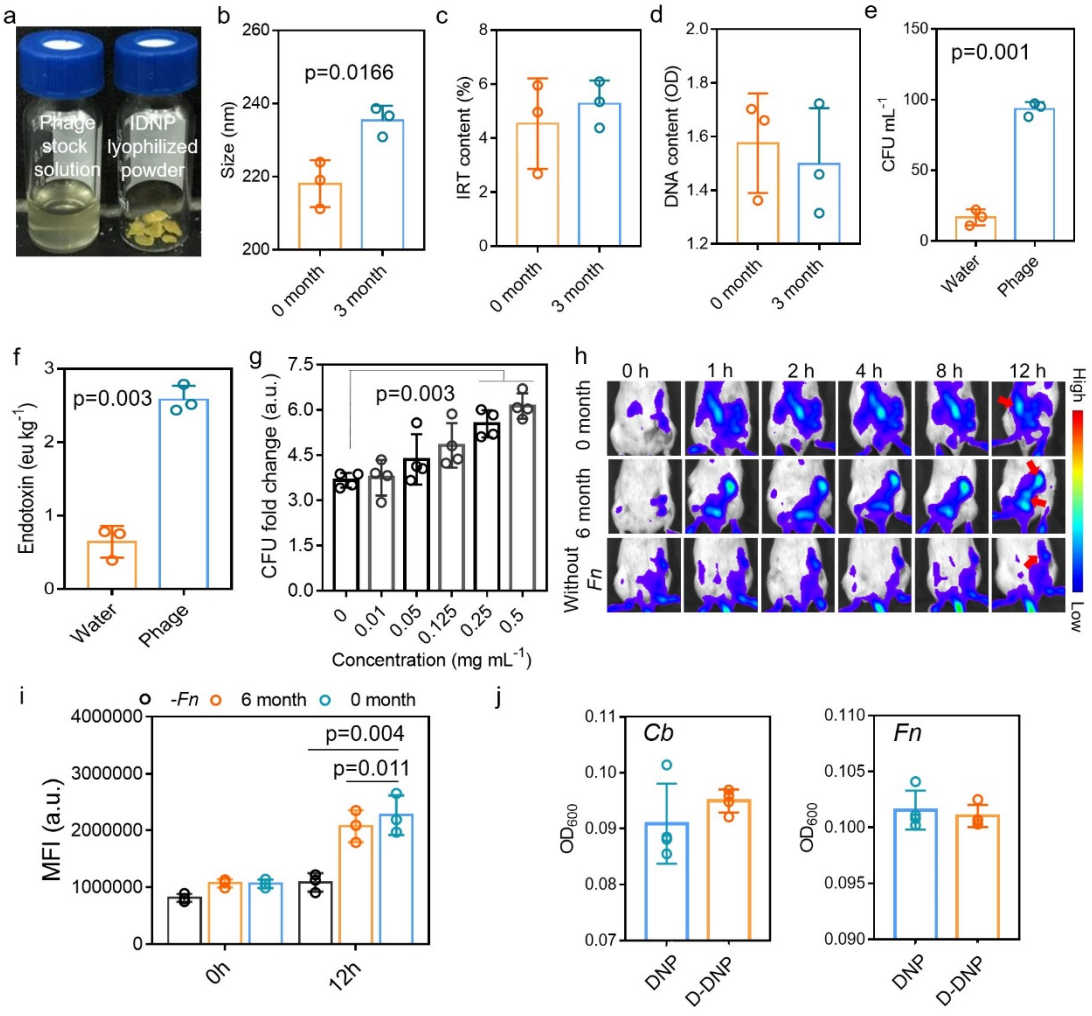

Supplementary Fig. 8 | The stability of bio/abiotic hybrid nano-system. (**a**) Images of phage stock solution (disperse in TBS) and DNP lyophilized powder. These samples were refrigerated at 4 ^{o}C for 3 month. (**b**) Particle size of DNP before and after 3 month of refrigeration. Three biological replicates are shown. (**c**) IRT content of IDNP before and after 3 month of refrigeration. Three biological replicates are shown. (**d**) DNA content in P2 phages before and after 3 month of refrigeration. Three biological replicates are shown. (**e**) and (**f**) Limulus test and colony count detection of phage stock solution and DNP lyophilized powder, respectively. Three biological replicates are shown. Both phages and DNP meet the standard of US FDA (K/M, *i.e.*,

5.0 eu/kg/maximum human/dose/kg administered in a single 1 h period; USP limit: < 10^2 CFU/mL). (**g**) Long-term storage (~ 6 months) of DNP nanoparticles did not affect its capacity in promoting *Cb* proliferation. Four biological replicates are shown. (**h**) Long-term storage (~ 6 months) of P2 phage did not affect its capacity in targeting orthotopic tumors of mice. The absence of tumor-colonized *Fn* restricted the tumor-targeting capacity of P2-phage. A representative image of three biological replicates is shown. Red arrows indicate orthotopic tumor positions. (**i**) Quantitative analysis for intratumoral accumulation of phage. Images were analyzed with Living Image software and the light intensity from the region of interest (ROI) corresponding to the tumor position was calculated. Three biological replicates are shown. (**j**) Effect of D-DNP and DNP on the proliferation of *Cb*. The functionalization of DNP did not change its biological effect towards *Cb* and *Fn*. Three biological replicates are shown. Significance between two groups was calculated by using two-tailed Student's t test (b, c, d, e). The mean values and S.D. are presented.

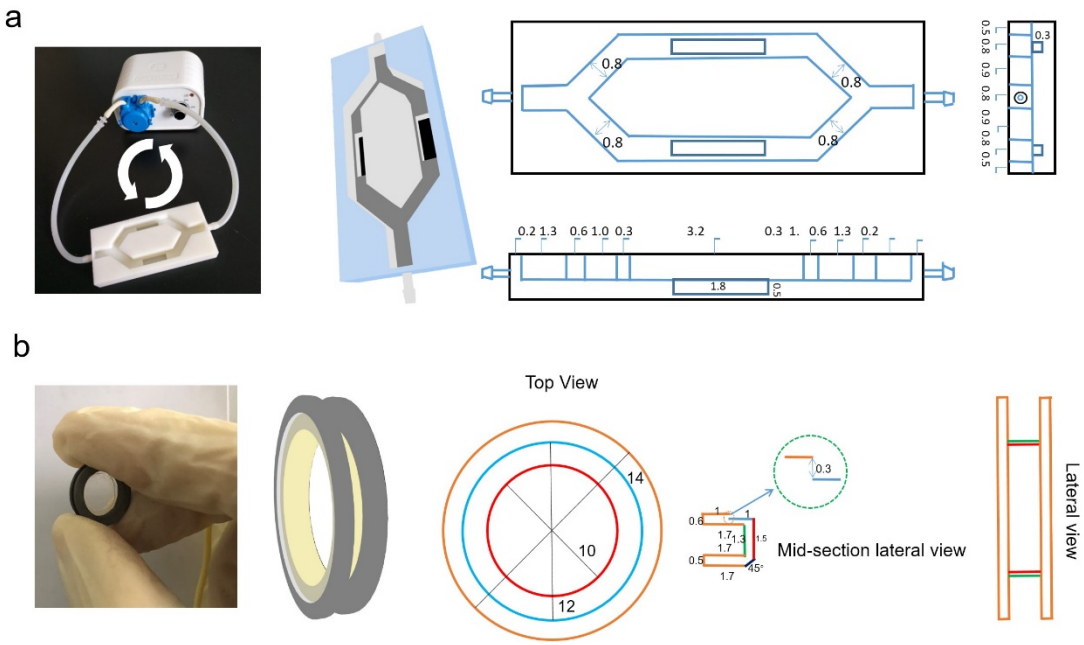

Supplementary Fig. 9 | Three View drawing of the circulating system and abdominal imaging window. (**a**) 3D and three views images of the circulating system. (**b**) 3D and three views images of abdominal imaging window.

Supplementary discussion 4. To study whether D-IDNP could be covalently linked to A-phage in a flow environment, we designed and fabricated a circulating system to simulate the condition of intestinal juice flow (Supplementary Fig. 9a). The simulated intestinal fluid with a viscosity of 35 cp was circulated at a speed of 0.85 cm s^{-1}. In this situation, rhodamine B labeled A-phage could still bind to FIT-labeled C *Fn*-immobilized hydrogel. Besides, IR808 conjugated D-IDNP was also added to this system, and remarkable accumulation could still be observed after the circulation.

To visualize the progress of orthotopic implanted colon cancer, an abdominal imaging window was fabricated and placed on the skin of abdomen (Supplementary Fig. 9b). Graefe forceps was used to place the abdominal wall and skin in the groove of this window. The window-implanted mice could be posited in an objective table with heating equipment and the orthotopic was observed with a stereomicroscope.

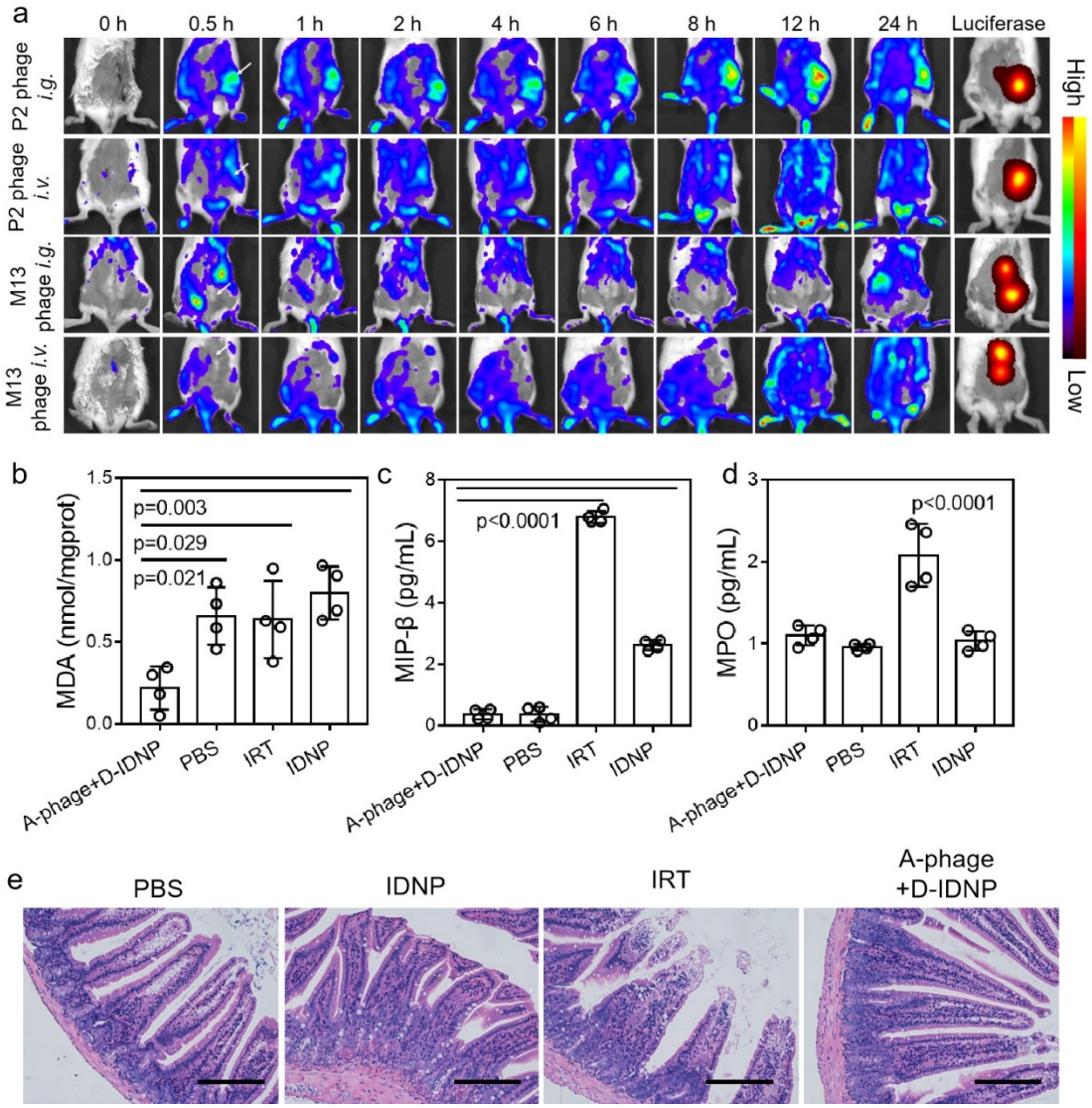

Supplementary Fig. 10 | The bioorthogonal reaction strategy for reducing side effects of chemotherapy. (**a**) The tumor targeting capacity of M13 or P2 phage contained nano-systems in CT26^{luc} bearing BALB/c mice tested by IVIS. Different administration methods including *i.v. or i.g.* were contrasted. M13 phages were used as a control. P2 phages by *i.g.* administration could be perfectly accumulated in CT26^{luc} tumors, indicating specific targeting of Fn. In contrast, M13 phages administration by *i.g.* or *i.v.* targeting *Fn* were randomly distributed among the intestinal tract. A representative image of three biological replicates is shown. White

arrows indicate tumor positions. (**b-d**) The content of inflammatory response factors (MIP-β, and MPO) and malondialdehyde (MDA) in colon tissues after treated with A-phage + D-IDNP, IRT or IDNP. A-phage + D-IDNP treatment showed low levels of inflammatory response factors compared with IRT treatment, indicating bioorthogonal reaction strategy could effectively reduce side effects of chemotherapy. Four biological replicates are shown. (**e**) H&E staining of BALB/c mice colon tissues after treated with A-phage + D-IDNP, IRT or IDNP. The intestinal mucosa after A-phage + D-IDNP treatment had a normal villi configuration. Five images per group were taken. Significance between two groups was calculated by using ANOVA with Tukey post hoc (b, c, d). The mean values and S.D. are presented.

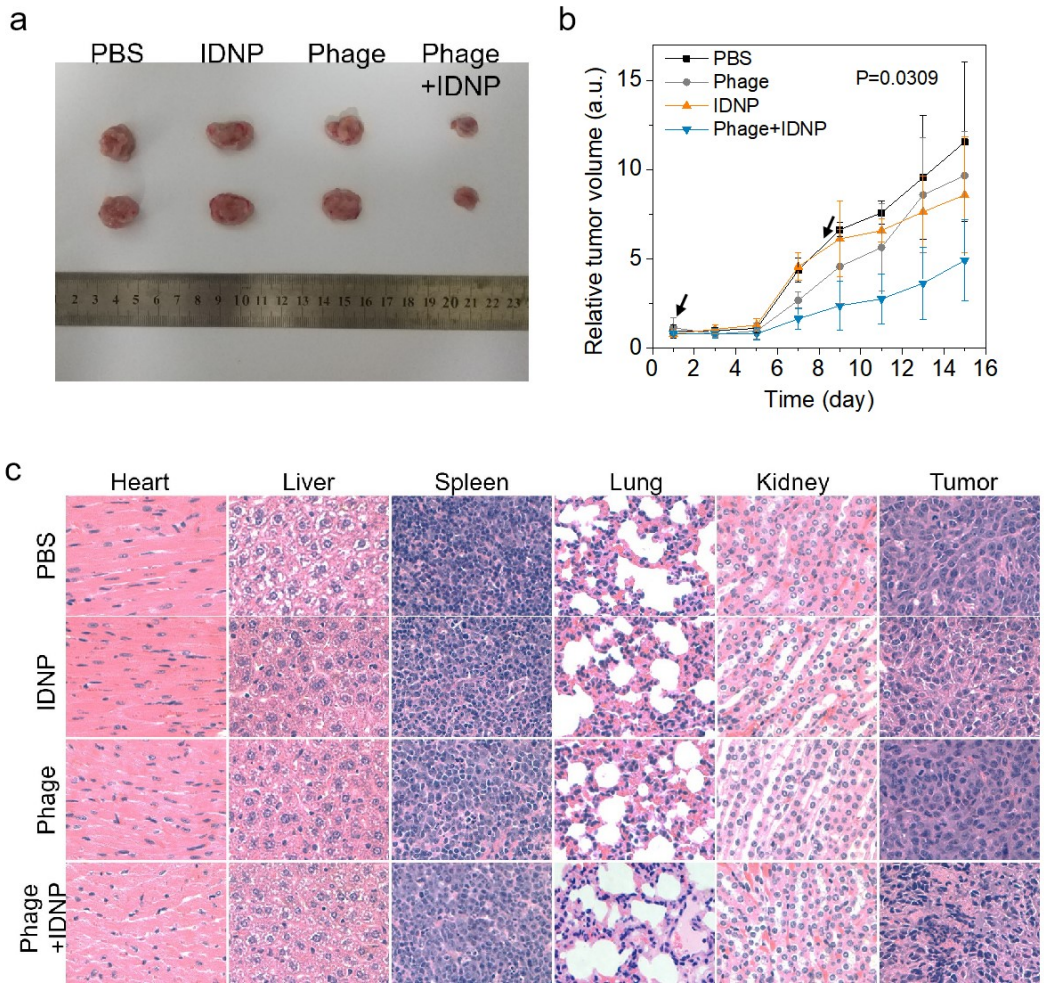

Supplementary Fig. 11 | Anti-cancer effect of bio/abiotic hybrid nano-system in subcutaneous tumor bearing mice. (**a**) Images of subcutaneous tumors collected from CT26 tumor bearing mice at the end of treatments. (**b**) Tumor volume curve of subcutaneous CT26 tumor bearing mice after receiving different treatments. Tumor volume curve and tumor images showed that phage + IDNP treatment displayed a higher tumor inhibition rate than other treatments. The arrow indicates the time for administration. Five biological replicates are shown. (**c**) H&E staining of tumor, heart, liver, spleen, lung and kidney collected from subcutaneous CT26 tumor bearing mice at the end of treatments. Five images per group were taken. Phage + IDNP treatment led to an enhanced amount of dead cells in the tumor tissue. In this subcutaneous

tumor model, both phages and IDNP were intratumorally injected into mice tumors. There is no need for considering the tumor targeting efficacy of chemotherapeutics. A-phage and D-IDNP were not tested in this experiment. Significance between two groups was calculated by using ANOVA. The mean values and S.D. are presented.

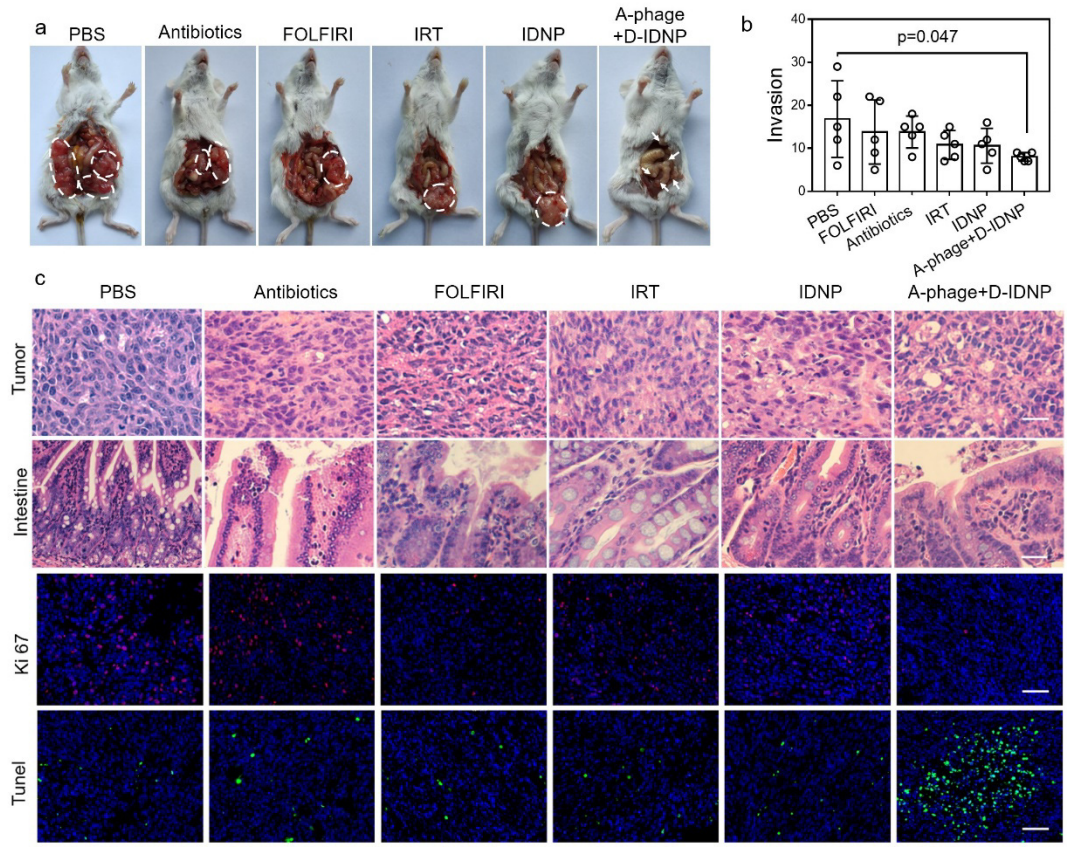

Supplementary Fig. 12 | Anti-cancer effect of phage-guided bio/abiotic hybrid nano-system on orthotopic CT26luc tumor bearing mice. (**a**) Images of colon tumors in orthotopic-tumor bearing mice after various treatments. A representative image of five biological replicates is shown. (**b**) Numbers of abdominal tumor metastasis in orthotopic-tumor bearing mice after various treatments. Five biological replicates are shown. Tumors were counted from mice sacrificed after the end of the experiment or mice that died in the experiment. Less macroscopical metastasis could be observed after the A-phage + D-IDNP treatment compared with other treatments, indicating the significant therapeutic efficacy in phage-guided bio/abiotic hybrid nano-system. (**c**) H&E staining, Ki67 staining and Tunel staining of primary colon cancer tissues in PBS, antibiotics cocktail, FOLFIRI, IRT, IDNP and A-phage +

D-IDNP treated mice. Five images per group were taken. The intestinal mucosa of orthotopic $CT26^{luc}$ tumor bearing mice that received A-phage + D-IDNP treatment showed less apoptosis or necrosis of crypts, and inflammatory cell infiltration. Longer villi could be observed in the intestinal tract of A-phage + D-IDNP treated mice. Immunofluorescence of Ki67 (red fluorescence) and TUNEL (green fluorescence) staining clearly showed prominent tumor suppression and irreversible cell apoptosis after A-phage + D-IDNP treatment. All above results demonstrated the remarkable anti-cancer effect of the phage-guided bio/abiotic hybrid nano-system.

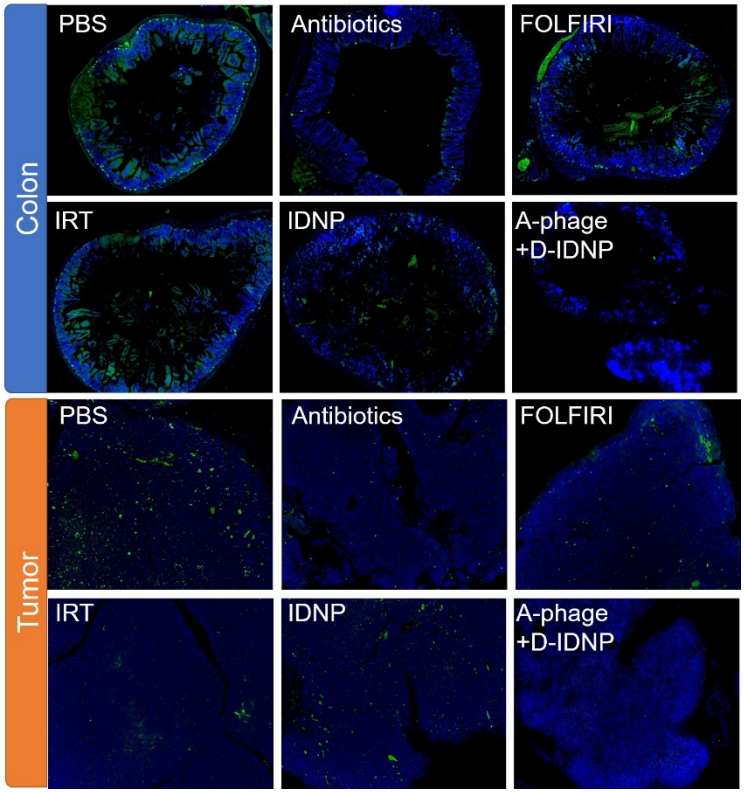

Supplementary Fig. 13 | Fluorescence images of *Fn* in tumors and colons of orthotopic-tumor bearing mice. *Fn* stained with a FISH probe (green fluorescence) could be found in tumor and colon tissue sections (n = 5 fields). A limited number of *Fn* could be observed in the tumors and colons of A-phage + D-IDNP treated group, which further proved specific elimination of A-phage.

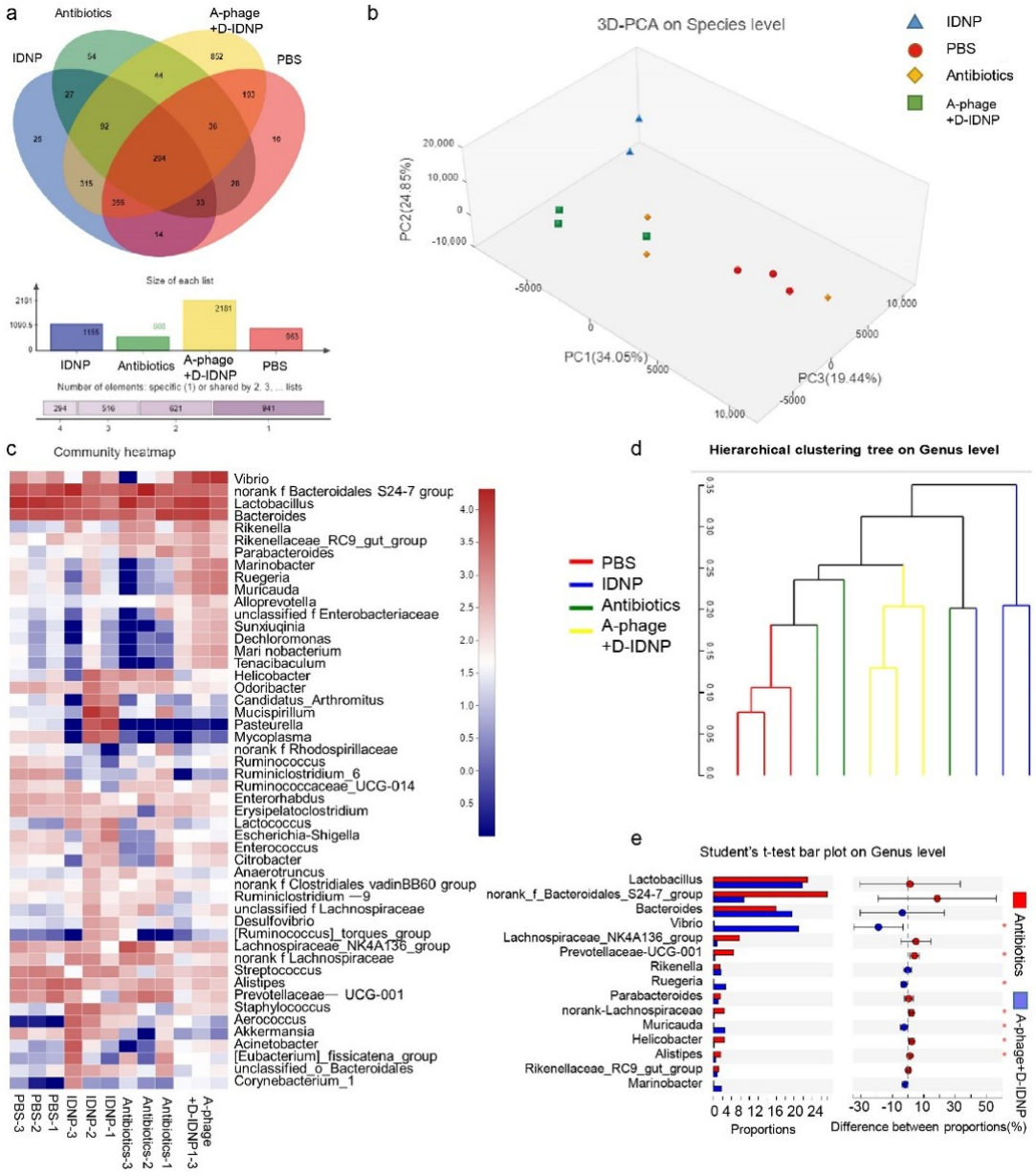

Supplementary Fig. 14 | Changes of gut microbes after A-phage + D-IDNP treatment. (**a**) Venn diagram of identified fecal bacterial strains in IDNP, antibiotic cocktail and A-phage + D-IDNP treated orthotopic-tumor bearing mice. A marked decrease of OTU abundance in antibiotic cocktail treated orthotopic CT26^{luc} mice was found. In contrast, A-phage + D-IDNP treatment improved the fecal OTU abundance. (**b**) 3D-PCA analysis of fecal microbiota compositions in IDNP, antibiotic cocktail and A-phage + D-IDNP treated orthotopic tumor-bearing mice. Three biological

replicates are shown. (**c**) Community heatmap of fecal microbiota compositions in IDNP, antibiotic cocktail and A-phage + D-IDNP treated orthotopic tumor-bearing mice. Three biological replicates are shown. (**d**) Hierarchical clustering analysis of fecal microbiota compositions NP, antibiotic cocktail and A-phage + D-IDNP treated orthotopic $CT26^{luc}$ tumor-bearing mice. Three biological replicates are shown. A similar gut microbiota signature could be found in A-phage + D-IDNP treated mice. This result suggested that the influence of this therapy towards the gut microbiota was stable. (**e**) Genus level analysis of significant difference bacterial species between different groups. Kruskal-Wallis H test was performed. Three biological replicates are shown.

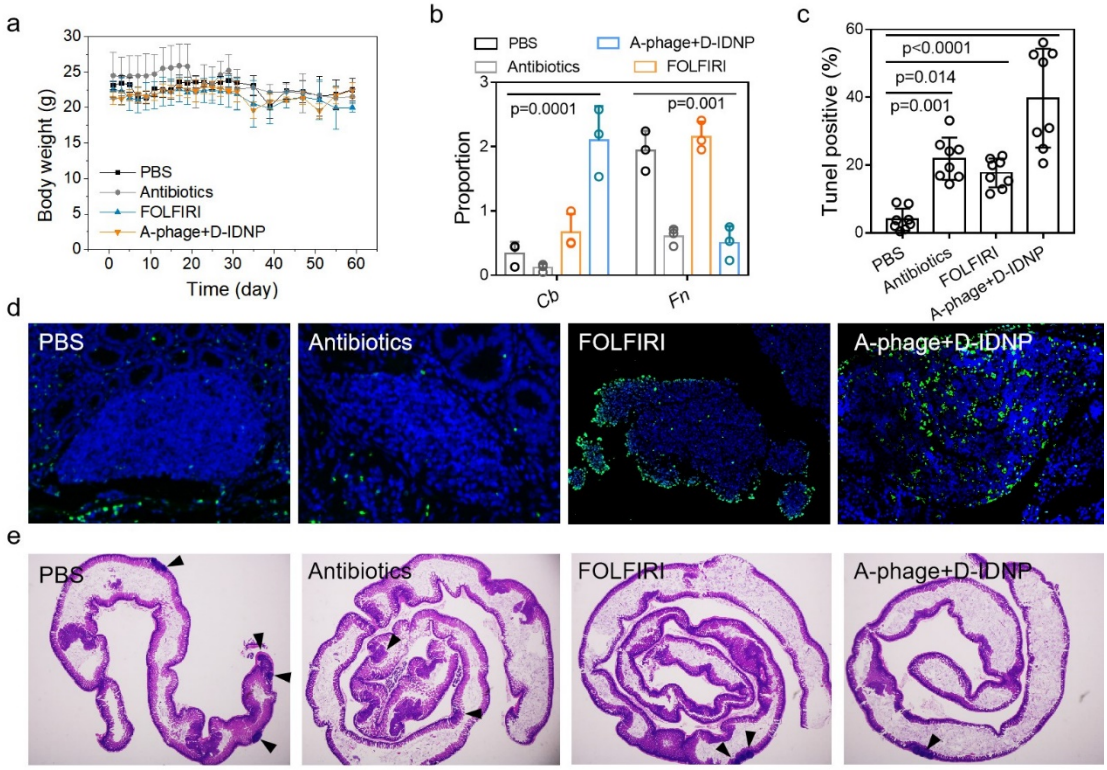

Supplementary Fig. 15 | Anti-cancer effect of A-phage + D-IDNP on ApcMin/+ mice. (**a**) Body weight curve of *Apc*$^{Min/+}$ mice under different treatments. Five biological replicates are shown. (**b**) PCR analysis of fecal *Fn* and *Cb* levels in PBS, antibiotic cocktail, FOLFIRI, and A-phage + D-IDNP treated *Apc*$^{Min/+}$ mice. Three biological replicates are shown. (**c**) Quantitative analysis of Tunel positive cancer cells in PBS, antibiotic cocktail, FOLFIRI, and A-phage + D-IDNP treated spontaneous tumors. Eight images per group were taken. (**d**) Tunel staining of intestinal polyps collected from PBS, antibiotic cocktail, FOLFIRI, and A-phage + D-IDNP treated *Apc*$^{Min/+}$ mice. Eight images per group were taken. (**e**) H&E staining of intestinal polyps collected from PBS, antibiotic cocktail, FOLFIRI, and A-phage + D-IDNP treated *Apc*$^{Min/+}$ mice. Five images per group were taken. Significance between two groups was calculated by using ANOVA (b) or ANOVA with Tukey post

hoc (c). The mean values and S.D. are presented.

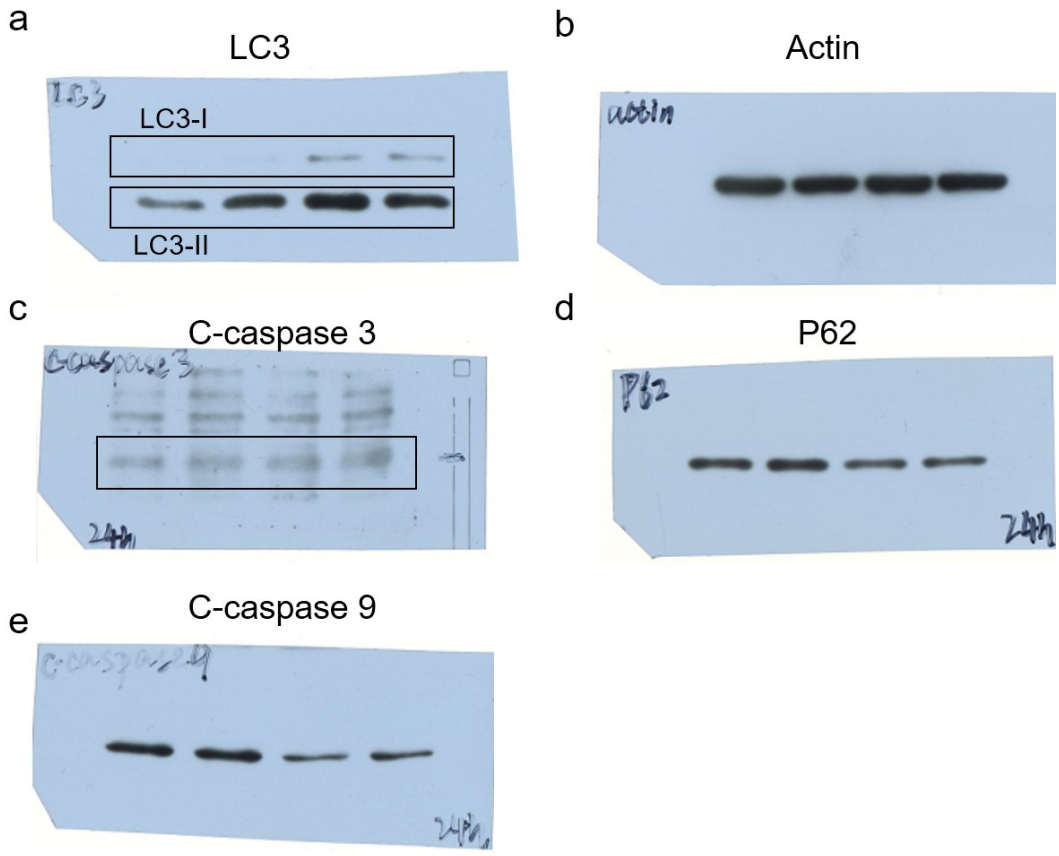

Supplementary Fig. 16 | Raw data for the western blot assay on the expression of cleavage caspase3, cleavage caspase9, P62, LC3-I, LC3-II and actin in CT26 cells.

CT26 cells were treated with PBS, IDNP, *Fn* + IDNP or *Fn* + IDNP + phage.

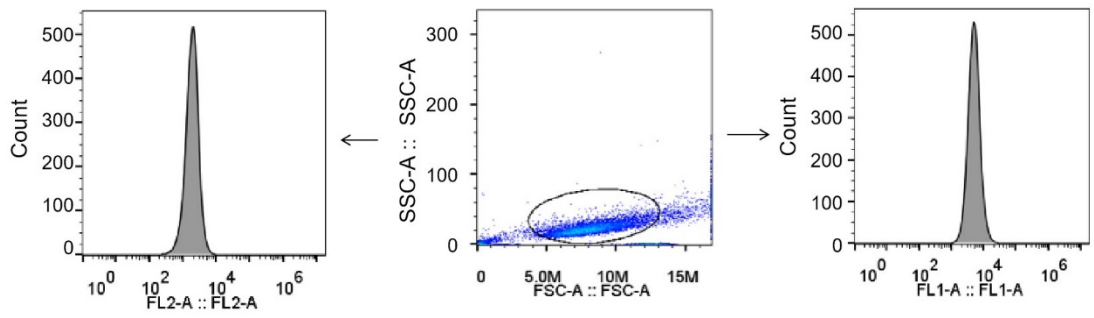

Supplementary Fig. 17 | Gating strategy for flow cytometry study. Cells were first gated on FSC-A/SSC-A. The fluorescence signals of GFP (FL1) and mCherry (FL2) were studied on this cell population.

Supplementary Table 1 | Gut microbiota in CRC patients and healthy individuals (genus level).

	Bacteria	*Clostridium*	*Fusobacterium*	*Eubacterium*	*Roseburia*
Control	75.52%	0.05%	0.12%	0.44%	3.21%
Control	81.17%	0.03%	0.01%	1.90%	0.62%
Control	80.51%	0.05%	0.01%	1.20%	0.57%
Control	73.15%	0.06%	0.01%	0.17%	0.76%
Control	49.96%	0.16%	0.01%	0.85%	5.24%
Control	43.07%	0.18%	0.01%	0.81%	4.36%
Control	74.19%	1.29%	0.32%	0.08%	0.14%
Control	95.13%	0.01%	0.01%	0.06%	0.29%
Control	60.49%	0.16%	0.01%	2.97%	3.87%
Control	53.84%	0.13%	0	0.09%	0.80%
Control	87.32%	0.08%	0.96%	1.60%	0.03%
Control	39.14%	0.35%	0.01%	0.74%	0.87%
Control	44.16%	0.26%	0.01%	0.56%	3.13%
Control	64.93%	0.05%	0.01%	1.18%	1.96%
Control	89.34%	0.03%	0.01%	0.02%	0.01%
Control	71.90%	0.25%	0.01%	0.43%	1.20%
Control	44.82%	0.3%	0.01%	2.21%	2.54%
Control	56.11%	0.12%	0.01%	1.42%	4.23%
Control	67.13%	0.52%	0	0.38%	0.60%
Control	28.53%	0.19%	0.01%	0.65%	0.90%
Control	45.42%	0.17%	0.01%	1.00%	4.64%
Control	51.75%	0.16%	0.01%	0.33%	5.60%
Control	57.99%	0.11%	0.01%	0.35%	2.13%
Control	38.66%	0.28%	0	2.06%	1.79%
Control	40.60%	3.16%	0.01%	1.34%	2.83%
Control	48.67%	4.67%	0.09%	0.32%	1.72%
Control	64.53%	0.59%	0.01%	0.28%	0.84%
Control	50.40%	0.19%	0.01%	2.22%	1.75%
Control	35.66%	0.24%	0.01%	0.94%	1.86%
Control	65.15%	0.41%	0.08%	2.08%	1.06%
Control	56.15%	0.41%	0.01%	1.96%	4.01%
Control	83.21%	0.06%	0.66%	0.07%	0.18%
Control	54.57%	0.15%	0.01%	4.84%	0.11%

Control	56.67%	0.16%	0.01%	2.08%	13.63%
Control	31.58%	0.37%	0.01%	1.07%	0.72%
Control	34.46%	0.32%	0.01%	0.71%	1.33%
Control	71.92%	1.32%	0.01%	0.18%	3.35%
Control	59.31%	0.14%	0.06%	1.02%	0.44%
Control	72.65%	0.44%	0.01%	1.42%	1.61%
Control	37.68%	0.27%	0.01%	0.96%	1.07%
Control	48.08%	0.19%	0.01%	3.41%	1.04%
Control	29.55%	0.19%	0.01%	2.41%	0.96%
Control	48.05%	0.46%	0.01%	0.71%	1.33%
Control	70.40%	0.75%	0.01%	0.45%	0.62%
Control	60.34%	0.08%	0.01%	3.27%	2.87%
Control	64.61%	0.19%	0.01%	0.21%	5.76%
Control	37.36%	0.47%	0.01%	1.51%	0.35%
Control	33.27%	0.14%	0.01%	1.08%	1.23%
Control	51.23%	0.42%	0.01%	0.26%	2.19%
Control	57.72%	0.09%	0.01%	0.43%	0.50%
Control	70.75%	0.17%	0.01%	0.64%	0.17%
Control	62.12%	0.19%	0.01%	3.58%	1.43%
Case	42.66%	0.76%	0.01%	0.68%	0.26%
Case	49.51%	0.22%	0.21%	1.59%	2.25%
Case	36.16%	0.16%	0.05%	0.54%	0.69%
Case	42.94%	0.18%	0.02%	0.41%	0.20%
Case	79.30%	0.06%	0.01%	0.12%	0.13%
Case	50.68%	0.18%	0.01%	0.75%	0.13%
Case	71.79%	0.09%	0.14%	0.12%	0.61%
Case	74.38%	0.05%	0.09%	0.18%	1.82%
Case	63.76%	0.07%	0.01%	3.00%	0.80%
Case	57.23%	0.26%	0.76%	0.14%	1.54%
Case	72.15%	0.22%	0.04%	0.11%	0.07%
Case	43.54%	0.41%	0.01%	0.42%	1.41%
Case	71.45%	0.12%	0.01%	0.21%	0.35%
Case	83.07%	0.03%	0.01%	0.13%	0.32%
Case	77.74%	0.04%	3.75%	0.18%	0.46%
Case	71.83%	0.08%	1.12%	0.01%	0.01%
Case	36.17%	0.13%	0.01%	0.17%	2.37%
Case	69.17%	0.10%	0.2%	0.04%	1.95%
Case	85.22%	0.03%	0.01%	0.37%	0.08%
Case	74.10%	0.63%	0.03%	0.14%	0.02%
Case	39.21%	0.26%	0.13%	0.22%	0.92%

Case	47.90%	0.40%	0.01%	0.85%	1.90%
Case	63.30%	0.24%	0.01%	0.70%	0.75%
Case	82.20%	0.07%	0.46%	0.16%	0.26%
Case	56.30%	0.27%	0.01%	1.49%	1.26%
Case	57.90%	0.74%	0.04%	0.15%	0.63%
Case	50.87%	0.11%	0.02%	0.19%	0.91%
Case	83.96%	0.05%	5.24%	0.14%	0.62%
Case	45.05%	0.21%	0.01%	0.64%	3.54%
Case	37.08%	0.49%	0.01%	0.16%	0.89%
Case	41.22%	0.47%	0.12%	0.52%	0.19%
Case	26.57%	0.19%	0.26%	0.55%	0.94%
Case	62.22%	0.23%	0.02%	0.43%	0.27%
Case	31.24%	0.09%	0.01%	0.65%	2.04%
Case	39.00%	0.44%	0.01%	0.73%	3.66%
Case	43.38%	0.32%	0.01%	0.54%	5.66%
Case	33.43%	0.72%	0.01%	0.5%	0.89%
Case	50.77%	0.15%	0.21%	0.22%	1.53%
Case	82.17%	0.25%	1.11%	0.03%	0.51%
Case	77.94%	0.11%	0.40%	0.27%	0.17%
Case	46.03%	0.29%	0.06%	1.79%	2.60%
Case	44.72%	0.16%	0.01%	1.33%	0.77%
Case	73.07%	0.25%	0.01%	0.93%	1.18%
Case	51.28%	0.29%	0.05%	0.15%	1.00%
Case	60.44%	0.14%	0.05%	0.37%	1.19%
Case	79.35%	0.15%	0.02%	0.10%	4.69%
Case	56.87%	0.22%	0.27%	1.10%	1.25%
Case	80.72%	0.11%	0.18%	1.27%	0.16%
Case	55.86%	0.14%	0.07%	0.12%	0.18%
Case	77.52%	0.13%	0.25%	0.16%	0.04%
Case	83.27%	0.16%	0.42%	0.02%	0.23%
Case	39.38%	0.23%	0.09%	0.35%	0.49%
Case	67.03%	0.14%	0.04%	0.26%	0.69%
Case	43.50%	0.80%	0.12%	0.23%	2.07%
Case	46.45%	0.08%	0.01%	1.17%	1.18%
Case	43.42%	0.43%	0.14%	0.32%	0
Case	56.24%	0.18%	0.01%	0.12%	0.10%
Case	76.06%	0.09%	0.60%	2.88%	1.74%
Case	53.71%	0.41%	0.13%	0.29%	0.37%
Case	56.77%	0.91%	0.01%	0.91%	0.60%
Case	81.16%	0.04%	0.45%	0.04%	0.71%

Case	50.29%	0.45%	0.01%	0.19%	0.77%
Case	59.32%	0.11%	0.01%	1.84%	9.25%
Case	49.63%	0.14%	0	0.58%	3.17%
Case	54.04%	0.17%	0.09%	1.64%	2.00%
Case	71.81%	0	0.01%	0	0
Case	61.10%	0.14%	0.28%	0.34%	1.12%
Case	51.23%	0.17%	0.03%	0.19%	0.18%
Case	48.17%	0.20%	0.01%	1.04%	1.06%
Case	94.48%	0.01%	0.01%	0.07%	0.01%
Case	55.86%	0.07%	0.07%	0.04%	0.01%
Case	66.75%	0.14%	0.01%	0.24%	0%

Supplementary Table 2 | Gut microbiota in CRC patients and healthy individuals (specie level).

	Bacteria	*Clostridium butyricum*	*Fusobacterium nucleatum*	*Eubacterium hallii*	*Roseburia intestinalis*
Control	75.52%	0.01%	0.01%	0.01%	1.23%
Control	81.17%	0	0.01%	0.03%	0.01%
Control	80.51%	0.01%	0	0.06%	0.01%
Control	73.15%	0	0	0.13%	0.01%
Control	49.96%	0.01%	0.01%	0.15%	0.34%
Control	43.07%	0.01%	0.01%	0.08%	0.08%
Control	74.19%	0.01%	0.01%	0.01%	0.08%
Control	95.13%	0	0.01%	0.03%	0.01%
Control	60.49%	0.01%	0	0.38%	0.23%
Control	53.84%	0.01%	0	0.06%	0.03%
Control	87.32%	0.01%	0.01%	0.01%	0.01%
Control	39.14%	0.01%	0	0.27%	0.09%
Control	44.16%	0.01%	0.01%	0.12%	0.53%
Control	64.93%	0	0.01%	0.08%	0.03%
Control	89.34%	0	0.01%	0.01%	0.01%
Control	71.90%	0.01%	0.01%	0.01%	0.16%
Control	44.82%	0.01%	0.01%	0.21%	0.58%
Control	56.11%	0.01%	0	0.03%	0.61%
Control	67.13%	0.01%	0.01%	0.06%	0.06%
Control	28.53%	0.01%	0.01%	0.09%	0.16%
Control	45.42%	0.01%	0.01%	0.04%	0.27%
Control	51.75%	0.01%	0.01%	0.06%	2.36%
Control	57.99%	0.01%	0.01%	0.03%	0.12%
Control	38.66%	0.01%	0	0.02%	0.04%
Control	40.60%	0.01%	0.01%	0.09%	0.06%
Control	48.67%	0.01%	0.03%	0.13%	0.02%
Control	64.53%	0	0.01%	0.19%	0.02%
Control	50.40%	0.01%	0.01%	0.17%	0.70%
Control	35.66%	0.01%	0.01%	0.36%	1.03%
Control	65.15%	0.01%	0.01%	0.01%	0.02%
Control	56.15%	0.01%	0.01%	0.06%	0.42%
Control	83.21%	0.01%	0.01%	0.01%	0.10%
Control	54.57%	0	0.01%	0.11%	0.02%

Control	56.67%	0	0.01%	0.01%	0.40%
Control	31.58%	0	0	0.61%	0.19%
Control	34.46%	0.01%	0	0.12%	0.35%
Control	71.92%	0.01%	0.01%	0.02%	1.82%
Control	59.31%	0.01%	0.01%	0.10%	0.02%
Control	72.65%	0.01%	0.01%	0.03%	0.46%
Control	37.68%	0.01%	0	0.10%	0.14%
Control	48.08%	0.01%	0.01%	0.06%	0.05%
Control	29.55%	0.01%	0	0.07%	0.08%
Control	48.05%	0.01%	0.01%	0.04%	0.06%
Control	70.40%	0.01%	0	0.01%	0.08%
Control	60.34%	0.01%	0.01%	0.07%	1.03%
Control	64.61%	0	0.01%	0.03%	0.05%
Control	37.36%	0.01%	0	0.02%	0.13%
Control	33.27%	0.01%	0.01%	0.06%	0.14%
Control	51.23%	0.01%	0.01%	0.15%	0.03%
Control	57.72%	0.01%	0.01%	0.01%	0.22%
Control	70.75%	0	0.01%	0.05%	0.05%
Control	62.12%	0.01%	0.01%	0.18%	0.49%
Case	42.66%	0.01%	0.01%	0.40%	0.04%
Case	49.51%	0	0.16%	0.08%	0.13%
Case	36.16%	0.01%	0.01%	0.47%	0.01%
Case	42.94%	0	0.01%	0.10%	0.01%
Case	79.30%	0	0.01%	0.06%	0.02%
Case	50.68%	0	0.01%	0.56%	0.01%
Case	71.79%	0	0.01%	0.01%	0.51%
Case	74.38%	0.01%	0.01%	0.02%	0.03%
Case	63.76%	0	0	0.04%	0.02%
Case	57.23%	0.01%	0.02%	0.04%	0.13%
Case	72.15%	0.01%	0.01%	0.01%	0.03%
Case	43.54%	0	0.01%	0.23%	0.03%
Case	71.45%	0.01%	0.01%	0.1%	0.04%
Case	83.07%	0	0.01%	0.01%	0.01%
Case	77.74%	0.01%	0	0.05%	0.20%
Case	71.83%	0.01%	0.01%	0.01%	0.01%
Case	36.17%	0	0.01%	0.12%	0.04%
Case	69.17%	0.01%	0.03%	0.01%	1.01%
Case	85.22%	0	0.01%	0.09%	0.01%
Case	74.10%	0.01%	0.01%	0.01%	0.01%
Case	39.21%	0.01%	0.05%	0.04%	0.02%

Case	47.90%	0.01%	0.01%	0.15%	0.15%
Case	63.30%	0.01%	0.01%	0.40%	0.05%
Case	82.20%	0.01%	0.01%	0.01%	0.03%
Case	56.30%	0.01%	0.01%	0.1%	0.38%
Case	57.90%	0	0.01%	0.07%	0.04%
Case	50.87%	0.01%	0.01%	0.04%	0.07%
Case	83.96%	0	0.01%	0.05%	0.02%
Case	45.05%	0	0.01%	0.07%	0.04%
Case	37.08%	0.01%	0.01%	0.04%	0.01%
Case	41.22%	0.01%	0.02%	0.03%	0.03%
Case	26.57%	0.01%	0.01%	0.11%	0.05%
Case	62.22%	0.01%	0.01%	0.03%	0.02%
Case	31.24%	0.01%	0.01%	0.02%	0.13%
Case	39.00%	0	0.01%	0.09%	0.04%
Case	43.38%	0.01%	0.01%	0.43%	0.08%
Case	33.43%	0	0.01%	0.01%	0.13%
Case	50.77%	0	0.11%	0.03%	0.03%
Case	82.17%	0.01%	0.2%	0.01%	0.01%
Case	77.94%	0	0.01%	0.01%	0.09%
Case	46.03%	0.01%	0.01%	0.31%	0.07%
Case	44.72%	0.01%	0	0.05%	0.04%
Case	73.07%	0.01%	0.01%	0.73%	0.03%
Case	51.28%	0.01%	0.01%	0.02%	0.01%
Case	60.44%	0.01%	0.03%	0.04%	0.03%
Case	79.35%	0.02%	0.01%	0.01%	4.46%
Case	56.87%	0.01%	0.01%	0.01%	0.06%
Case	80.72%	0.01%	0.01%	0.01%	0.10%
Case	55.86%	0.01%	0.01%	0.01%	0.02%
Case	77.52%	0.01%	0.01%	0.03%	0.01%
Case	83.27%	0.01%	0.06%	0.01%	0.01%
Case	39.38%	0.01%	0.01%	0.04%	0.04%
Case	67.03%	0.01%	0.01%	0.02%	0.01%
Case	43.50%	0.01%	0.03%	0.05%	0.14%
Case	46.45%	0.01%	0.01%	0.02%	0.05%
Case	43.42%	0.01%	0.07%	0.22%	0
Case	56.24%	0.01%	0.01%	0.07%	0.03%
Case	76.06%	0.01%	0.02%	0.01%	0.55%
Case	53.71%	0.01%	0.01%	0.04%	0.05%
Case	56.77%	0.01%	0.01%	0.03%	0.15%
Case	81.16%	0	0.01%	0.02%	0.01%

Case	50.29%	0.01%	0	0.04%	0.02%
Case	59.32%	0.01%	0.01%	0.05%	1.89%
Case	49.63%	0.01%	0	0.01%	0.05%
Case	54.04%	0.01%	0.01%	0.17%	0.82%
Case	71.81%	0	0.01%	0	0
Case	61.10%	0.01%	0.01%	0.03%	0.04%
Case	51.23%	0.01%	0.01%	0.02%	0.02%
Case	48.17%	0.01%	0.01%	0.05%	0.61%
Case	94.48%	0.01%	0	0.01%	0.01%

Supplementary Table 3 | Abbreviation of LEfSe analysis.

Letter	Taxa
d	g__Lachnoclostridium
e	s__Clostridium_sp__40cc_B_5824_ARE
f	s__unclassified_g__Lachnoclostridium
g	s__Clostridium_fusiformis
h	s__uncultured_organism_g__Lachnoclostridium
i	g__Lachnospiraceae_UCG_010
j	s__uncultured_bacterium_g__Lachnospiraceae_UCG_01
k	s__Lachnospiraceae_bacterium_COE1
l	s__Blautia_coccoides_g__Lachnospiraceae_NK4A136_g
m	s__unclassified_g__Roseburia
n	g__Anaerostipes
o	s__unclassified_g__Anaerostipes
p	g__Lachnospiraceae_UCG_001
q	s__unclassified_g__Lachnospiraceae_UCG_001
r	s__mouse_gut_metagenome_g__norank
s	s__Clostridium_sp__ASF356
t	s__Lachnospiraceae_bacterium_DW46
u	s__unclassified_g__Lachnospiraceae_UCG_006
v	g___Eubacterium__fissicatena_group
w	s__unclassified_g___Eubacterium__fissicatena_grou
x	g___Ruminococcus__gauvreauii_group
y	s__Ruminococcus_gauvreauii
z	s__unclassified_g__Blautia
a1	f__Family_XIII
b1	g___Eubacterium__brachy_group
c1	s__uncultured_bacterium_g___Eubacterium__brachy_
d1	g__Family_XIII_UCG_001
e1	s__uncultured_bacterium_g__Family_XIII_UCG_001
f1	f__Peptostreptococcaceae
g1	g__Romboutsia
h1	s__uncultured_bacterium_g__Romboutsia
i1	g__Ruminococcus_1
j1	s__unclassified_g__Ruminococcus_1
k1	g__Ruminiclostridium_6
l1	s__uncultured_bacterium_g__Ruminiclostridium_6
m1	g__Ruminiclostridium_5
n1	s__unclassified_g__Ruminiclostridium_5
o1	s__uncultured_bacterium_g__Ruminiclostridium_5
p1	s__uncultured_Clostridiales_bacterium_g__Ruminic
q1	s__Clostridiales_bacterium_CIEAF_026
r1	g__Ruminococcaceae_UCG_010

s1	s__uncultured_bacterium_g__Ruminococcaceae_UCG_0
t1	s__uncultured_organism_g__Ruminococcaceae_UCG_01
u1	s__uncultured_bacterium_g__Anaerotruncus
v1	s___Clostridium__leptum_g__Anaerotruncus
w1	g__Ruminiclostridium
x1	s__unclassified_g__Ruminiclostridium
y1	s__uncultured_bacterium_g__Ruminiclostridium
z1	g__Butyricicoccus
a2	s__uncultured_bacterium_g__Butyricicoccus
b2	s__unclassified_g__Butyricicoccus
c2	g__Ruminococcaceae_NK4A214_group
d2	s__uncultured_bacterium_g__Ruminococcaceae_NK4A2
e2	s__uncultured_Clostridiales_bacterium_g__Ruminoc
f2	g__Ruminococcus_2
g2	s__unclassified_g__Ruminococcus_2
h2	f__Clostridiaceae_1
i2	g__Candidatus_Arthromitus
j2	s__Candidatus_Arthromitus_sp__SFB_mouse_Japan
k2	g__Clostridium_sensu_stricto_1
l2	s__unclassified_g__Clostridium_sensu_stricto_1
m2	s__Lactobacillus_murinus_g__Lactobacillus
n2	s__Lactobacillus_intestinalis
o2	c__Negativicutes
p2	o__Selenomonadales
q2	f__Acidaminococcaceae
r2	g__Phascolarctobacterium
s2	s__uncultured_organism_g__Phascolarctobacterium
t2	g__Erysipelatoclostridium
u2	s__Erysipelatoclostridium_ramosum
v2	s___Clostridium__cocleatum
w2	g__Faecalibaculum
x2	s__uncultured_bacterium_g__Faecalibaculum
y2	g___Clostridium__innocuum_group
z2	s__uncultured_bacterium_g___Clostridium__innocuu
a3	g__Turicibacter
b3	s__Turicibacter_sp__LA61
c3	g__Faecalitalea
d3	s__unclassified_g__Faecalitalea
e3	g__norank_f__Erysipelotrichaceae
f3	s__uncultured_bacterium_g__norank_f__Erysipelotr
g3	g__Coprobacillus
h3	s__Coprobacillus_cateniformis
i3	s__uncultured_Barnesiella_sp__g__norank
j3	s__uncultured_organism_g__norank_f__Bacteroidale

k3	f__Porphyromonadaceae
l3	g__Odoribacter
m3	s__uncultured_bacterium_g__Odoribacter
n3	g__Parabacteroides
o3	g__Rikenellaceae_RC9_gut_group
p3	s__unclassified_g__Rikenellaceae_RC9_gut_group
q3	s__uncultured_bacterium_g__Rikenellaceae_RC9_gut
r3	s__unclassified_g__Rikenella
s3	g__Alloprevotella
t3	s__uncultured_Bacteroidales_bacterium_g__Allopre
u3	f__Bacteroidaceae
v3	g__Bacteroides
w3	s__uncultured_Bacteroidales_bacterium_g__Bactero
x3	s__Bacteroides_acidifaciens
y3	s__Bacteroides_sp__I48
z3	c__Alphaproteobacteria
a4	o__Rhodospirillales
b4	f__Rhodospirillaceae
c4	g__norank_f__Rhodospirillaceae
d4	s__gut_metagenome_g__norank_f__Rhodospirillaceae
e4	c__Deltaproteobacteria
f4	o__Desulfovibrionales
g4	f__Desulfovibrionaceae
h4	g__Bilophila
i4	s__uncultured_bacterium_g__Bilophila
j4	g__Desulfovibrio
k4	s__unclassified_g__norank_o__Gastranaerophilales
l4	g__Parvibacter
m4	s__uncultured_bacterium_g__Parvibacter
n4	g__unclassified_f__Coriobacteriaceae
o4	s__unclassified_f__Coriobacteriaceae
p4	s__unclassified_g__Enterorhabdus
q4	g__Coriobacteriaceae_UCG_002
r4	s__uncultured_bacterium_g__Coriobacteriaceae_UCG
s4	o__Bifidobacteriales
t4	f__Bifidobacteriaceae
u4	g__Bifidobacterium
v4	s__Bifidobacterium_pseudolongum_PV8_2

Supplementary Table 4 | GOC categories of differential genes associated pathways. I: Information storage and processing, C: Cellular processes and signaling, M: Metabolism, P: Poorly characterized.

Type	Functional categories	PBS *vs* RT COG	PBS *vs* IRTNOG	PBS *vs* Fn COG	PBS *vs* Fn NOG	PBS *vs* Phages COG	PBS *vs* Phages NOG
I	[A] RNA processing and modification	2	9	4	22	4	18
I	[B] Chromatin structure and dynamics	30	12	33	17	22	5
I	[J] Translation, ribosomal structure and biogenesis	26	7	44	15	29	11
I	[K] Transcription	28	93	29	111	22	103
I	[L] Replication, recombination and repair	33	11	39	12	30	9
C	[D] Cell cycle control, cell division, chromosome partitioning	23	9	16	8	14	7
C	[M] Cell wall/membrane/envelope biogenesis	9	1	12	1	9	0
C	[O] Posttranslational modification, protein turnover, chaperones	64	128	87	157	67	126
C	[T] Signal transduction mechanisms	40	76	61	95	57	79
C	[U] Intracellular trafficking, secretion, and vesicular transport	24	138	29	224	23	191

C	[V] Defense mechanisms	7	0	10	0	7	0
C	[Y] Nuclear structure	0	0	0	0	1	0
C	[Z] Cytoskeleton	39	25	45	34	43	37
M	[C] Energy production and conversion	31	2	40	4	28	4
M	[E] Amino acid transport and metabolism	28	2	42	1	32	1
M	[F] Nucleotide transport and metabolism	17	2	30	3	21	2
M	[G] Carbohydrate transport and metabolism	33	4	40	6	32	5
M	[H] Coenzyme transport and metabolism	11	0	17	0	16	0
M	[I] Lipid transport and metabolism	27	18	39	27	31	24
M	[P] Inorganic ion transport and metabolism	22	6	32	7	30	4
M	[Q] Secondary metabolites biosynthesis, transport and catabolism	19	1	25	2	17	1
P	[R] General function prediction only	154	236	175	314	172	255
P	[S] Function unknown	19	275	33	386	32	338

Supplementary Table 5 | Size and zeta potential of various materials.

Materials	Size	Zeta potential
AuNP	58 nm	-19.7 mV
AgNP	49 nm	-14.9 mV
Fe_3O_4 NP	95 nm	-17 mV
C_3N_4 NP	310 nm	1.99 mV
Cellulose nanocrystal	60 nm	-20.1 mV
Graphene nanosheet	Planar size: 1-3 μm, thickness: 1-5 nm	-5.68 mV
ZnO NP	80 nm	0.682 mV
DNP	310 nm	-2.89 mV

Supplementary Table 6 | Information of tissue microchip. Patients were staged according to the sixth edition of the UICC/AJCC TNM staging

Number	Sex	Age	Position	Tumor type	T	N	M	TNM stage
A1,2	Female	53	Rectum	Adenocarcinoma	T2	N0	M0	I
A3,4	Female	63	Colon transversum	Mucinousadenocarcinoma	T3	N0	M0	IIA
A5,6	Male	70	Ileocecum	Adenocarcinoma	T2	N0	M0	I
A7,8	Male	64	Sigmoid	Adenocarcinoma	T3	N0	M0	IIA
A10,B8	Male	67	Ascending colon	Adenocarcinoma	T3	N0	M0	IIA
B1,2	Female	71	Right hemicolon	Adenocarcinoma	T3	N0	M0	IIA
B3,4	Male	39	Sigmoid	Adenocarcinoma	T4	N0	M0	IIB
B5,6	Female	63	Rectum	Adenocarcinoma	T4	N0	M0	IIB
B7,A9	Male	51	Ascending colon	Adenocarcinoma	T4	N2	M0	IIIC
B9,10	Male	56	Left hemicolon	Mucinousadenocarcinoma	T3	N0	M0	IIA
C1,2	Male	62	Rectum	Adenocarcinoma	T4	N1	M0	IIIB

C3,4	Female	52	Rectum	Tubular adenoma carcinogenesis	T1	N1	M0	IIIA
C5,6	Male	62	Rectum	Tubulo-villous adenoma	T2	N0	M0	I
C7,8	Male	61	Rectum	Adenocarcinoma	T3	N1	M0	IIIB
C9,10	Female	50	Right hemicolon	Adenocarcinoma	T3	N0	M0	IIA
D1,2	Female	72	Rectum	Adenocarcinoma	T3	N2	M0	IIIC
D3,4	Male	52	Sigmoid	Adenocarcinoma	T4	N1	M1	IV
D5,6	Male	66	Sigmoid	Adenocarcinoma	T2	N1	M0	IIIA
D7,8	Male	41	Sigmoid	Adenocarcinoma	T3	N0	M0	IIA
D9,10	Female	61	Rectum	Adenocarcinoma	T2	N0	M0	I
E1,2	Male	56	Rectum	Adenocarcinoma	T2	N0	M0	I
E3,4	Female	68	Ileocecum	Adenocarcinoma	T3	N1	M0	IIIB
E5,6	Male	71	Ileocecum	Mucinousadenocarcinoma	T3	N0	M0	IIB
E7,8	Male	66	Rectum	Adenocarcinoma	T3	N0	M0	IIA
E9,10	Female	72	Rectum	Adenocarcinoma	T3	N0	M0	IIA
F1,2	Male	86	Sigmoid	Adenocarcinoma	T3	N1	M0	IIIB
F3,4	Male	59	Ileocecum	Adenocarcinoma	T3	N0	M0	IIB
F5,6	Male	52	Rectum	Adenocarcinoma	T3	N0	M0	IIB
F7,8	Male	81	Rectum	Adenocarcinoma	T3	N2	M0	IIIC

F9,10	Male	43	Ascending colon	Adenocarcinoma	T3	N2	M0	IIIC
G1,2	Male	60	Rectum	Adenocarcinoma	T3	N0	M0	IIA
G3,4	Male	62	Ascending colon	Adenocarcinoma	T4	N2	M0	IIIC
G5,6	Female	51	Rectum	Mucinousadenocarcinoma	T2	N1	M0	IIIA
G7,8	Female	50	Rectum	Adenocarcinoma	T2	N0	M0	I
G9,10	Female	53	Right hemicolon	Mucinousadenocarcinoma	T4	N2	M0	IIIC